AAPT PHYSICS EDUCATION | AMERICAN JOURNAL of PHYSICS

Quantum electrical transport in samples of limited dimensions

D. F. Holcomb

Citation: Am. J. Phys. **67**, 278 (1999); doi: 10.1119/1.19251
View online: http://dx.doi.org/10.1119/1.19251
View Table of Contents: http://ajp.aapt.org/resource/1/AJPIAS/v67/i4
Published by the American Association of Physics Teachers

Quantum electrical transport in samples of limited dimensions

D. F. Holcomb
Department of Physics and Laboratory of Atomic and Solid State Physics, Cornell University, Ithaca, New York 14853

(Received 13 July 1998; accepted 29 September 1998)

The ability to make electrically conducting structures of ever smaller size by nanofabrication techniques (the playground of *mesoscopic physics*) has brought with it entry into a wonderful new range of unexpected quantum phenomena. Interpretation of these phenomena requires full recognition of the wave nature of electrons and requires keeping track of the phase coherence of the electron wave functions and/or the discreteness of electron energy levels in samples of interest. Happily, many of the phenomena can be observed through the use of very straightforward experimental probes—commonly the dc electrical conductivity or conductance, and the Hall effect. The phenomena are observed in samples with one or more dimensions comparable to either the electron wavelength (up to 40 nm for carriers at the Fermi energy in some semiconductors) or the inelastic scattering length of the carriers (as large as many microns in some systems at low temperatures). Ohm's law is no longer a firm guide to current–voltage relationships, and the Drude–Sommerfeld picture of electrical conduction is superseded. Many of the interesting phenomena are seen in samples of either two-dimensional (i.e., a third dimension is of the order of or less than the electron wavelength) or one-dimensional nature (either a tight, short constriction in the conductor or a longer ''quantum wire''). In certain one-dimensional structures, one may have ballistic transport between input and output connections, and the quantum character of the electron motion is fully displayed. Planck's constant h appears in the characteristic quantum of electrical conductance, e^2/h. In two dimensions, the addition of a large magnetic field produces the remarkably deep and still somewhat mysterious Quantum Hall Effect, characterized by the quantum of resistance, $R_K=h/e^2=25812.8\,\Omega$. Other examples of the observation of electron interference and diffraction phenomena *within* solid materials are briefly highlighted. This short tutorial treatment emphasizes observed phenomena rather than details of the theoretical structures used to interpret them.

TABLE OF CONTENTS

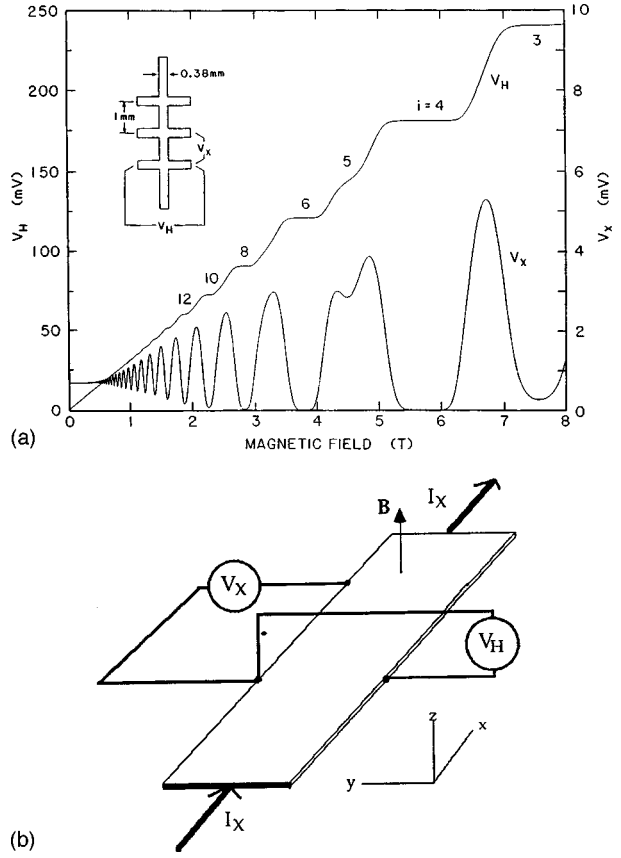

Fig. 1. (a) Chart recordings of voltages V_H and V_x [see (b)] as a function of B_z for a GaAs–AlGaAs heterojunction at $T=1.2$ K. Source–drain current I_x is 25.5 mA, charge density in the 2D electron layer, $n_A=5.6\times10^{11}$ cm^{-2}. [From M. E. Cage, R. F. Dziuba, and B. F. Field, IEEE Trans. Instrum. Meas. **IM-34**, 301 (1985) © IEEE, reproduced by permission.] (b) Model experimental setup for acquiring data such as shown in (a).

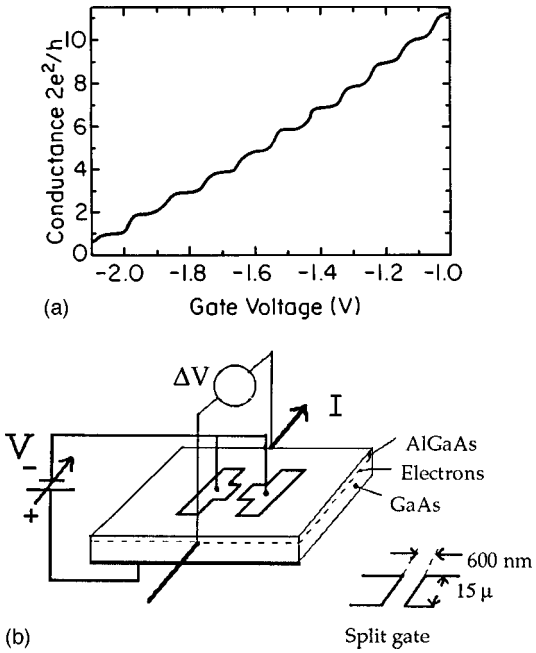

Fig. 2. (a) Data for electrical conductance, $G=I/\Delta V$, of the structure shown in (b), as a function of gate voltage, V. (Data taken from Ref. 2.) (b) Sketch of typical experimental setup used to acquire data such as shown in (a). The ''split-gate'' geometry was introduced by Thornton *et al.* (Ref. 14).

I. INTRODUCTION AND MOTIVATION

Discovery of the Quantum Hall Effect (QHE) in 1980[1] by von Klitzing, Dorda, and Pepper signaled the arrival of a new era in the study of the fundamentals of electron transport in electrical conductors. A new combination of fundamental constants of nature appeared. In certain two-dimensional (2D) conductors (that is, systems in which the third dimension of the system is of the order of or smaller than the Fermi wavelength λ_F), the Hall resistance, R_{xy}, if measured as a function of magnetic field B or as a function of areal carrier density n_A, was found to have the staircase structure shown in Fig. 1(a). These measurements were made with the experimental setup represented in Fig. 1(b). The values of R_{xy} in the flat regions of the ''treads'' in Fig. 1(a) were found to be described by the relationship

$$R_{xy}\equiv V_H/I_x=\frac{h}{ie^2}=\frac{25\,812.80}{i}\,\Omega, \tag{1}$$

where i takes integral values. Many experimental measurements of R_{xy} tell us that the quantum factor h/e^2 in this relationship is *exact*, that is, R_{xy} is fully determined by the fundamental constants h and e.

The second remarkable feature of Fig. 1(a) is the form of $R_{xx}=V_x/I_x$ as a function of B. This longitudinal resistance is evidently vanishingly small over the ranges of B in which the value of R_{xy} lies in the flat region of a step.

The cascading growth of techniques to produce *mesoscopic* systems, systems in which one or more dimensions is of the order of or smaller than the Fermi wavelength, or the elastic scattering length of the carriers, $l_{\rm el}$, or both, led to an explosion of experimental studies of new phenomena in which the quantum wave nature of electrons plays an essential role. We are now directly observing electron interference and diffraction effects *inside* a bulk conductor—a new realm of observation.

In mesoscopic systems in which electron transport is confined to a *single* dimension (achieved through the fabrication of narrow constrictions or of ''quantum wires''), the e^2/h combination was observed, in the form of quantized levels of conductance in these one-dimensional (1D) systems. Figure 2(a) is an example of the relevant observations published in 1988 by two groups, one at the Phillips Research Laboratories[2] and one at the Cavendish Laboratory in Cambridge.[3] In these measurements, there is no magnetic field applied. Figure 2(b) sketches the experimental arrangement needed to generate the required 1D constriction in electron flow pattern. It was found that the electrical conductance, G, of these 1D transmission systems is given by the quantum relationship

$$G=m2e^2/h, \tag{2}$$

where m is again an integer. In studies to date, this relationship has not been found to have the clean precision of the fundamental QHE relationship, Eq. (1). The apparent reasons for this failure to experimentally realize the perfect integral quantum relationship of Eq. (2) are discussed in Sec. III B.

A variety of experiments in three-dimensional (3D) materials as well as in the lower dimensional samples demonstrate directly the wave nature of the electron, by means of observation of interference and diffraction effects. In this paper, we touch on the 3D manifestations only briefly.

The stance of this paper is fundamentally a phenomenological one. I will focus on descriptions of the experimental findings and the explanation thereof in terms of models which are consistent with currently accepted theory, but will frequently stop short of a full exploration of the nuances. It is assumed that the reader has a working knowledge of models of the behavior of electrons in metallic conductors and semiconductors, at the level of Kittel's text.[4] For a deeper study of topics treated herein, the reader will be, from time to time, directed to one of several original research papers (selected from the, literally, hundreds which have been published), suitable technical reviews, or monographs.[5,6] Many of these references, as well as several hundred other papers, appear in the fully annotated compendium of references in the 1990 Resource Letter[7] by C. T. Van Degrift and M. E. Cage.

One might well ask, ''Why now?'' What features of the modern, mesoscopic systems and modern experimental techniques have prepared the way for exploration of this new regime of electron transport phenomena? Here are some important ones.

(1) The semiconducting materials (primarily silicon and gallium arsenide) upon which the world of mesoscopic physics rests have several intrinsic properties which favor observation of quantum effects. Mobile electrons in these materials have long Fermi wavelengths which bring quantum phenomena to the fore more easily than in ordinary metals. These materials can be prepared in states of high chemical purity and relatively perfect lattice structure. The high carrier mobilities required for observation of a number of the effects which I will treat depend on such relatively perfect materials.

(2) These basic effects are much enhanced by the modern experimental techniques of fabricating materials layer by layer in a fully controlled fashion. With suitable external voltage-gating techniques, the electrons can be confined to layers with several critical properties—thickness comparable to the mobile electron wavelengths, reduced scattering to encourage the exceedingly large mobilities required for observation of several effects, and control of carrier concentrations by an external ''knob,'' the voltage gate.

(3) Another factor of importance in some cases is the accessibility of experimental temperatures in the 10-mK–1-K range made possible by the modern ^{3}He–^{4}He dilution refrigerator. A number of the phenomena of interest are quickly obscured if thermal excitations or thermally encouraged scattering plays a significant role.

For mesoscopic samples with varying geometries and different arrangements for attachment of electrical leads, fascinating quantum interference phenomena, including manifestations of the Aharonov–Bohm effect, are found. In studies of samples of ''zero dimensions'' (i.e., all three dimensions of a sample comparable to or smaller than the electron wavelength, λ_F), the ''quantum dot'' field arose. In this paper, I shan't treat either of these last two sets of phenomena. Webb and Washburn have given[8] a very nice tutorial discussion of the Aharonov–Bohm phenomena. Study of the quantum dot systems focuses primarily on distributions of electron energy levels or on intersystem electron transport, rather than transport within the material itself. Thus the study of the quantum dot systems falls somewhat outside the purview of this paper. A short introduction to the matter of energy levels has been given by McEuen[9] and a full review of the matter of electron transport into and out of quantum dots can be found in an article by Kouwenhoven *et al.*[10]

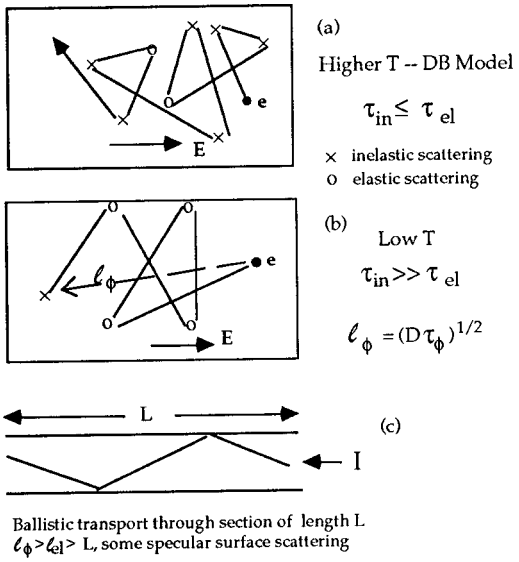

Fig. 3. Three types of electrical conduction characteristic of particular length-scale relationships. (a) Conventional Drude–Sommerfeld conduction in a metal at moderate temperatures. $\tau_{in} < \tau_{el}$. (b) At low temperatures, quantum interference effects appear when $\tau_{in} \gg \tau_{el}$, and $l_\phi = (D\tau_\phi)^{1.2}$. (c) Ballistic transport through a section of length L. $l_\phi > l_{el} > L$. There is some specular surface scattering.

II. BACKGROUND

Review of models of electron transport: (1) The *Drude–Sommerfeld model.* In order to establish a well-defined starting point, we review briefly certain key features of the Drude–Sommerfeld model of electrical conduction in metallic systems.[11] In this model, assuming a single relaxation time τ and associated mean free path l for the scattered carriers, we can write an expression for the electrical conductivity σ,

$$\sigma = ne\mu = ne^2\frac{\tau}{m^*} = g\left(e^2\frac{\tau}{m^*}\frac{k_F^3}{6\pi^2}\right) = g\left(\frac{e^2}{h}\frac{k_F}{3\pi}\right)k_F l, \tag{3}$$

where n and μ have their usual significance. In the last form of the expression, quantum mechanics appears as a result of the transformation of the term $n\tau/m^*$ to its appropriate equivalent for a system of free electrons governed by the Pauli principle. k_F is the Fermi wave vector, g is a degeneracy factor. (When one has degeneracy, more electrons can be packed into the volume of k space characterized by $k < k_F$. In the simplest case, $g=2$ to allow for the two electron spin directions.)

In my discussion, particularly in Secs. III and V, the distinction between elastic scattering (no energy loss by the electron, hence preservation of $|\mathbf{k}|$ and retention of wave function phase information) and inelastic scattering (energy exchange with lattice, phase scrambling) will be important, particularly at low temperatures where $\tau_{\text{inelastic}} \gg \tau_{\text{elastic}}$. Figure 3 displays a cartoon which may assist in sensing the transition from the realm of the Drude–Sommerfeld picture, first to the quantum world in which full attention to electron wave phenomena is important and ultimately to the world of ballistic transport—no electron phase breaking between current injection contact and current extraction contact.[12]

(2) *Characteristic length scales.* Observability of many of the phenomena of interest in both the 2D systems (Quantum

Table I. Typical relevant lengths and other data in several 3D and 2D systems.[a]

Property	Copper	GaAs inversion layer	Si MOSFET
Fermi wavelength	0.46 nm	40 nm	35–112 nm
Electron mobility	50 $cm^2/V\,s$ (300 K)	$\approx 10^6$ $cm^2/V\,s$	10^4 $cm^2/V\,s$
mfp $\boldsymbol{l}=v_F\tau$		10^2-10^4 nm	10^2 nm
Phase coherence length $\boldsymbol{l}_\phi=(D\tau_\phi)^{1/2}$		Uncertain	40–400 nm (1 K)
Cyclotron radius, $\frac{\hbar k_F}{eB}$ (at $B=10$ T)	9×10^3 nm	10 nm	4–12 nm (depends on n_A, controlled by gate voltage)
Magnetic length $\boldsymbol{l}_B=(h/eB)^{1/2}$		8 nm (at $B=10$ T)	
Electron effective mass	$\approx m_e$	$0.07m_e$	$0.2m_e$

[a]Most data for GaAs and Si MOSFET taken from Table I, p. 7 of Ref. 6.

Hall Effect) and 1D (quantized conductance) systems is controlled by the relationships among a number of different length scales which will characterize the regime in which various effects are observed. The length scales of interest are

- dimensions of the sample—L,w,t,
- wavelength of electrons at the Fermi surface, λ_F,
- the elastic scattering length for the carriers, $l_{\rm el}$,
- the phase coherence length for the carriers,

$$\boldsymbol{l}_\varphi=(D\tau_\varphi)^{1/2},$$

where D (the overall diffusion constant) $=v_F^2\tau/2$, and $\tau_\varphi=\tau_{\rm in}$ is the phase coherence time, the time between inelastic scattering events. We are implicitly working in a regime in which $\tau_{\rm in}\gg\tau_{\rm el}\cong\tau$, i.e., the situation shown in Fig. 3(b). Note that the idea of an inelastic scattering length, defined as $\boldsymbol{l}_{\rm in}=v_F\tau_{\rm in}$, is not useful in this regime. While this figure might evoke images of billiard ball scattering in the reader's mind, I emphasize that satisfactory models for phenomena treated in this paper require full consideration of wave properties of the electrons.

- The so-called ''magnetic length'' for the carriers, $l_B=(\hbar/eB)^{1/2}$.

(This magnetic length is the classical radius of an orbit of energy $\hbar\omega_c/2$, the ground state energy of the quantum cyclotron system.)

Table I gives values of some of these characteristic lengths for various materials.

With these five length scales at our disposal, we can identify relationships among them which are necessary in order to produce regimes within which phenomena of our interest are visible. These are tabulated in Table II.

III. 1D BALLISTIC CONDUCTION IN CONSTRICTIONS (REF. 13) AND QUANTUM WIRES

Figure 4 displays a schematized version of the split-gate arrangement of Fig. 2(b) with which data such as that of Fig. 2(a) are obtained. The thickness t describes a layer of electrons bound near the AlGaAs–GaAs interface shown in Fig. 2(b). The potential well at that interface (discussed in more detail in Sec. IV) captures the electrons in a quantum standing wave state so that their motion is limited to the 2D bowtie of Fig. 4. The further channeling of electron motion to the constriction of width w is forced by the negative potential on the split gate of Fig. 2(b). At values of w comparable to the Fermi wavelength of the electrons, standing wave states are established in that direction as well. We have then created a system with the traveling wave **k** vector restricted to the line running through the constriction—hence the waveguide analogy. The constriction forms a ''one-dimensional conductor.''

Table II. Effects of various length relationships.

Regime	Phenomenon	Comments
$L,w,t\gg\boldsymbol{l}\gg\lambda_F$	3D—ordinary Drude–Sommerfeld conductivity	
$L,w,t\gg\boldsymbol{l}\gg\lambda_F$ B large, $\omega_c\tau<1$	3D—ordinary Hall effect	
$L,w,t\gg\boldsymbol{l}\leqslant\lambda_F$ $B=0$	3D—strong scattering, Ioffe–Regel limit	Conductivity becomes diffusive (jump distance≈atom spacing) when $\boldsymbol{l}\leqslant\lambda_F$
$L,w,t\gg\boldsymbol{l}\gg\boldsymbol{l}_B\gg\lambda_F$ B large, $\omega_c\tau\gg1$	3D—quantum magnetotransport effects visible	For example, Schubnikov–de Haas, de Haas–van Alphen
$L,w,>\boldsymbol{l}\gg\lambda_F\approx t$ $B=0$	2D system, standing waves in z direction, ordinary D–S conductivity in 2D layer	Realized in Si MOSFETs, GaAs-GaAlAs layers
$L,w>\boldsymbol{l}\gg\lambda_F\approx t\gg\boldsymbol{l}_B$ (B large)	2D system, electron standing waves in the z direction, resolved Landau levels, realm of Integral Quantum Hall effect	Realized in Si MOSFETs, GaAs–GaAlAs layers
$\boldsymbol{l}_\phi\gg\boldsymbol{l}_{\rm el}\geqslant L\gg w\approx\lambda_F\approx t$ $B=0$	Ballistic transport in 1D, quantization of G, model of G a la Landauer	Realized in split-gate system, quantum wire, carbon nanotube

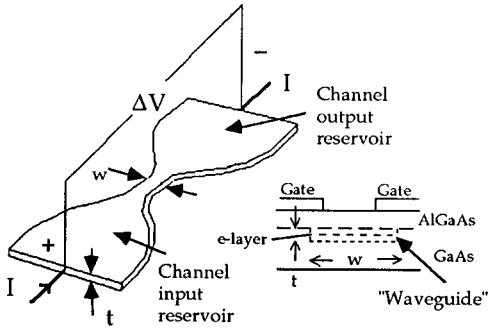

Fig. 4. Schematic picture of constriction in conduction electron occupancy of the interface layer in a GaAs/AlGaAs heterojunction, the constriction being formed by the setup shown in Fig. 2(b). Quantum conduction channels are formed in the constriction, with occupancy of successive waveguide modes controlled by the gate voltage V shown in Fig. 2(b).

We note that true ballistic transport through the constriction (i.e., no elastic scattering from defects) is required in order to observe the stair-step structure of Fig. 2(a).

Transport through the constriction of Fig. 4, measured by the conductance ratio $I/\Delta V$, generates the quantum conductance steps of magnitude $2e^2/h$ shown in Fig. 2(a). (The factor 2 represents the effect of the two degenerate spin states for each electron waveguide mode.) I emphasize that this phenomenon should be thought of as a quantization of *conductance* not conductivity. The term ''conductivity'' implicitly invokes the concept of a local property of a material which governs charge flow in response to a local electric field. The conductance G is the ratio $I/\Delta V$, where I is the total current in the constriction and ΔV the potential drop between entrance to and exit from the constriction.

A. ''Conduction as transmission''

Key to a satisfying model of the quantum conductance steps is a picture in which the 1D constriction or quantum wire is viewed as a waveguide for transmission of electron quantum waves between an entrance reservoir and an exit reservoir. The waveguide dimension t shown in Fig. 4 is set by the thickness of the electron layer in the GaAs/AlGaAs heterojunction and the width w is controlled by the voltage V applied to the split gate, shown in Fig. 2(b).

B. Quantization of *G*, the conductance

The waveguide picture is very naturally handled quantitatively by the ''conduction as transmission'' model, whose development rests (in a not very transparent fashion) on early work of R. M. Landauer.[14] We assume that the layer thickness t and electron density are such that only the lowest t-controlled energy band is occupied. In the transverse dimension, the width of the constriction is controlled by the gate voltage. Increasing that width generates additional laddered states with energies determined by the values of w and Fermi wavelength λ_F. The quantum conduction modes characterized by the two quantum numbers set by values of t and of gate voltage, respectively, are called ''channels.''

Figure 4 envisions a two-terminal measurement, in which ΔV is measured between an input reservoir which supplies current I to the constriction and an exit reservoir which extracts that current. *It is important to note that the conductance G is a property of the* assemblage *of input and output reservoirs and constriction. It is a* system *property, not a property of a particular material.*

1. A model for G

If we assign m as the quantum number of a particular channel in the waveguide, the current transmitted via that channel m can be expressed as

$$I_m = e v_m \left(\frac{dn}{dE}\right)_m \Delta\mu, \tag{4}$$

where v_m is the group velocity of an electron at the Fermi energy in channel m, $(dn/dE)_m$ is the appropriate density of states (per unit length) at this value of E_F (neglecting spin degeneracy for the moment), and $\Delta\mu$ is the difference in electrochemical potential between the channel input reservoir and the channel output reservoir. If we then write

$$\left(\frac{dn}{dE}\right)_m = \left(\frac{dn}{dk}\right)\left(\frac{dk}{dE}\right) = \frac{1}{2\pi}\frac{1}{\hbar v_m}, \tag{5}$$

Eq. (4) becomes

$$I_m = e\frac{1}{2\pi\hbar}\Delta\mu. \tag{6}$$

[In 1D, $(dn/dk) = 1/2\pi$.]

Establishing the value of $\Delta\mu$ by applying a voltage difference ΔV between the input and output reservoirs gives

$$I_m = \frac{e^2\Delta V}{2\pi\hbar}. \tag{7}$$

Thus

$$G_m = \frac{I_m}{\Delta V} = \frac{e^2}{2\pi\hbar} = \frac{e^2}{h}. \tag{8}$$

This derivation was made without regard to channel number m. If the electron density and channel width w are such that N waveguide channels are populated, the total conductance is

$$G = \left(\frac{2e^2}{h}\right)N \equiv NG_0. \tag{9}$$

The factor 2 has been inserted to count the two spin states which can be accommodated in each channel.

2. Observing the quantum conductance steps

We can now see what is going on in Fig. 2(a). A larger value of the negative voltage on the split gates squeezes the effective value of the width w (see Fig. 4) and, thus, depopulates the channels at larger quantum numbers. As that voltage is made less negative, as shown in Fig. 2(a), more and more channels are populated and the conductance G rises in integral steps as given in Eq. (2). We note that the uniform spacing of the quantized values of G arises from the fact that the density of states in a 1D system is the constant factor of $(1/2\pi)$ used in Eq. (6).

The arrangement suggested by the model of Fig. 4 is just one of a variety of physical structures that can be treated using the ''conduction as transmission'' picture introduced by Landauer. The relationship given above as Eq. (9) implicitly assumes smooth flow of current from supply reservoir through the constriction to the exit reservoir. More generally, G can be written as

$$G = \left(\frac{2e^2}{h}\right)\sum T_j, \tag{10}$$

where T_j is a transmission coefficient for injection of current into the jth of the N occupied channels.[15]

In experiments with the split-gate constrictions, how closely does the measured value of G match the quantum conductance factor $2e^2/h$? The data of Fig. 2(a) imply that the values of T_j are all unity for the particular sample structure shown in Fig. 2(b). Beenakker and van Houten[16] describe some of the reasons why the measured values may differ from the actual value of $2e^2/h$ by 1% or more. I list here some of the relevant factors.

(1) Electrons must enter and leave the constriction from and to subsystems in local equilibrium. In the idealized constriction of Fig. 4, the equilibration occurs seamlessly and there is no reflection at the entrance to the constriction,

whereas for a real system this reflection will occur, diminishing the conductance given by Eq. (9). Even with the adiabatic transmission of Fig. 4, extra voltage drops that result from the attachment of real voltage probes in the equilibrated regions at some distance from the constriction (as in Fig. 4) will add small iR drops to the value of ΔV in Eq. (9), giving a smaller measured value of the quantum factor e^2/h.

(2) The model of ballistic conduction (see Fig. 3) assumes specular reflection at the boundaries of the constriction. A small amount of backscattering may compromise the perfect conductance. If there is true ballistic conduction, the conductance should be independent of the length of the 1D section. Such is not found to be the case experimentally.

The arrangement sketched in Fig. 2(b) and the model of Fig. 4 represent a ''two-terminal'' arrangement in which current supply and voltage measurement use the same input–output connections. Equation (9) applies to such an arrangement. Reference 6, pp. 106–109, expands the discussion to include the four-terminal configuration, in which current leads and voltage measurement probes are separate.

Following the initial experiments with split-gate constrictions,[2,3] conductance steps have also been observed in a number of other systems.

(1) A longer (2 mm), more ''wirelike'' construction was contrived in the GaAs system by Yacoby *et al.*[17] by means of a very elaborate fabrication process. By application of several gate voltages, electrons were confined in two dimensions to form the ''wire.'' The conductance steps were generated by varying one of these gate voltages in order to control the number of occupied channels. The steps, however, occurred at conductance levels typically 15% less than the $2e^2-h$ quantum value. Such a result is not inconsistent with the picture we have been developing. Observation of the $2e^2/h$ quantum value requires perfect transmission ($T=1$) into the appropriate 1D channel. Imperfect transmission (or losses in the incoming leads in a two-terminal measurement) would be expected to lower the conductance. I think there is every reason to believe that the stairstep behavior reported in Ref. 17 arises from the same basic quantization of G seen in the split-gate configuration of Refs. 2 and 3.

(2) Conductance steps have been observed in extraordinarily fine gold wires[18] produced by a delicate separation of a gold tip from a gold film with which the tip is in contact. In another related but charmingly simple scheme,[19] steps have been observed in the conductance between two macroscopic wires in loose contact. The wires are made to separate by vibration of the assembly. The conductance between wires is monitored as a function of time in the course of breaking the contact, and is seen to exhibit downward steps of magnitude $2e^2/h$ as the wires separate.

(3) Most recently and most dramatically, the unit quantum conductance, $2e^2/h$, has been observed[20] in studies of conducting carbon ''nanotubes.''

Both of these latter experiments are, again, two-terminal measurements of the value of G, and thus subject to the small departures from G_0 that may appear as a consequence of losses in entering and departing electrical leads, or the departures from perfect ballistic transmission which may cause values of T_j in Eq. (10) to decrease slightly from unity.

C. A connection to optics

Historically, wave phenomena have been studied most extensively using electromagnetic waves in the optical wavelength region. The Phillips Labs group has taken seriously the search for optical analogs of the electron quantum wave phenomena which form the core of this article. For example, a description of the optical analog of the electron behavior shown in Fig. 2(a) is given in an article in *Nature*.[21]

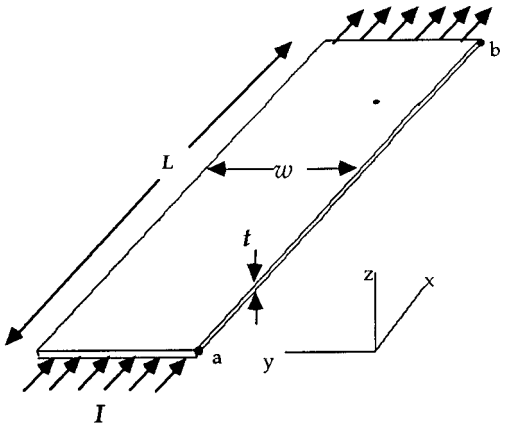

Fig. 5. Configuration of a 2D sample. The sketch defines symbols used in the text.

IV. THE ''INTEGRAL'' QUANTUM HALL EFFECT (IQHE)

A. Special characteristics of 2D systems

1. Homogeneous 2D conductors

Consider the thin plate sketched in Fig. 5. If it is a homogeneous 3D system, for current flowing as shown, the potential difference, V_{ab}, will be given by

$$V_{ab}=RI=\left(\rho\frac{L}{wt}\right)jwt, \tag{11}$$

where ρ is the resistivity and j is the current per unit cross-sectional area. If the current is constrained to a 2D flow pattern, the symbol j now represents the current per unit width. (In the systems of our interest, the constraint to 2D charge flow is imposed by the establishment of a quantum standing wave in the z direction, when $t\leqslant\lambda_F$.) Thus

$$V_{ab}=RI=\left(\frac{\rho_{2D}L}{w}\right)jw. \tag{12}$$

The resistivity ρ_{2D} now has the dimensions of ohms and is usually called ''the resistance per square.'' This phrase reflects the fact that for a 2D system, the resistance of *any* square of the material, regardless of its size, is ρ_{2D}. (In a square conductor of side L, as L increases, increase in the current path length L is just balanced by a wider transport path, and the resistance is independent of the value of L.) For a homogeneous 2D sample of length L and width w, the resistance R is given by $R=\rho_{2D}L/w$.

In a two-dimensional conductor (with **k** vectors restricted to the $x-y$ plane), Eq. (3) becomes

$$\sigma_{2D}=n_Ae\mu=n_Ae^2\frac{\tau}{m^*}=g\frac{e^2}{h}\frac{k_Fl}{2}. \tag{13}$$

(Carrier density per unit area is n_A.) The significance of the combination of fundamental constants, e^2/h, is highlighted

in the 2D case. In a ''good'' conductor, we will have the condition $k_F l \gg 1$, and for a very poor conductor, $k_F l \leqslant 1$. Thus we see that the boundary between ''good'' and ''poor'' conductors is marked by the quantum conductance factor, e^2/h. Note that the quantity σ_{2D} has units (ohm^{-1}) and is, thus, a conductance. That is,

$$\sigma_{2D} = G = \frac{(\text{total current})}{\Delta V}.$$

2. Localization of charge carriers in 2D systems

In 1979, Abrahams, Anderson, Licciardello, and Ramakrishnan (AALR)[22] put forward a provocatively sweeping theoretical model of the behavior of G, the electrical conductance of a disordered conductor in the $T=0$-K limit. Its conclusions are particularly relevant to electron transport processes in 2D and 1D, a primary subject of this paper. In particular, AALR concluded that for a 2D system at $T=0$ K, with no magnetic field present, the conductance of a square of side, L, $G(L)$, would decrease exponentially with L at sufficiently large values of L. That is,

$$G(L) \propto e^{-L/L_0},$$

where L_0 is, thus, a *localization length*. (Remember that in a conventional picture of a homogeneous 2D conductor, G is a fixed number for a square of *any* dimension.)

From a simple, geometrical point of view, a qualitative difference between the 3D and 2D situations is not too surprising. Paths of electron escape from a scattering event are more restricted for conduction in the 2D plane.

This prediction of AALR has taken a prominent place in discussion of G_{2D} and has provoked many experimental tests. A very recent set of experiments with Si metal-oxide-semiconductor field-effect transistors (MOSFETS) of particularly high quality (mobility $\mu > 3\times10^4$ cm^2/V s) reported by Kravchenko *et al.*[23] shows G approaching a constant value as the temperature T nears 0 K and gives a strong suggestion that for such real materials the prediction of AARL is not borne out. (However, it is wise to remind ourselves that all experimental samples have an upper limit to L set by the sample dimensions. One cannot rigorously exclude the possibility that the localization length L_0 is large compared to the sample dimensions.) A provocative note from this work of Kravchenko *et al.* is that the dividing line in conductance between samples which are metallic as $T \to 0$ K and those which are insulating is

$$G \cong 0.5 e^2/h.$$

The characteristic scale for quantum conductance, e^2/h, again appears.

I emphasize that both the AARL model and the experimental results of Kravchenko *et al.* treat situations with $B \cong 0$. We'll note later that a large magnetic field is expected to alter the localization properties.

3. Physical realization of 2D systems

There are two prime systems in which the 2D electron system has been neatly generated and intensively studied, the Si MOSFET and the GaAs/Al_xGa_{1-x}As heterostructure. Treatments of these systems are found in a number of sources.[24] I remind the reader of their configuration and properties with the sketches of Fig. 6. In the Si MOSFET, the carrier electron system is confined to a 2D layer in the Si device by an electric field perpendicular to the Si base. A potential well of roughly triangular shape is formed at the SiO_2–Si interface, within which the required quantized energy levels are created. This 2D layer is a so-called ''inversion layer,'' in which the free charges are electrons, even though the doping of the Si is nominally p type. In the AlGaAs/GaAs heterostructure, a similar, roughly triangular well is formed in the GaAs layer. In this case, the electric field which generates the inversion layer in the GaAs is generated internally as a consequence of the different band gaps for GaAlAs and GaAs and the appropriate doping of AlAs (donors) and GaAs (acceptors). Modulation doping of AlGaAs places impurity scattering centers well back from the inversion layer, giving the very high mobilities in the GaAs heterostructure.

4. Electronic subbands in 2D systems

The triangular potential well generated in the Si MOSFET or in the GaAlAs/GaAs interface restricts electron travel to the 2D space. Figure 6(c) gives a qualitative picture of the relevant quantum levels. The fundamental physics is that of an electron contained in a 1D box, even though the shape of the wave functions generated by a calculation of the energy levels in the triangular potential is obviously different. The lowest ''standing wave'' state is occupied at low electron concentration. Higher energy levels are reached either by packing more electrons into the layer or by an appropriate form of excitation. The different energy levels provide the so-called ''subbands'' seen in various quantum conduction or optical phenomena. (We use the term ''bands'' because the **k** vector of the electrons may still range over k_x–k_y space without constraint.)

B. Effects of magnetic fields in 2D (Ref. 25)

With the addition of a magnetic field **B** to a driving electric field **E**, the charge carriers feel the Lorentz force, $\mathbf{F} = e[\mathbf{E} + (\mathbf{v}\times\mathbf{B})]$. An obvious consequence is the appearance of circular, interscattering, paths of cyclotron radius

$$R_c = \frac{p}{eB} = \frac{\hbar k_F}{eB},$$

with a cyclotron frequency

$$\omega_c = \frac{eB}{m^*}. \tag{14}$$

k_F is the wave number of a carrier at the Fermi surface of the relevant conductor and m^* is the effective mass of the carriers.

At low temperatures the scattering time τ can be sufficiently long that $\omega_c \tau \gg 1$. In that case, well-defined cyclotron levels are formed. Quantization of these cyclotron levels gives the energy equation,

$$\frac{\hbar^2}{2m^*}(k_x^2 + k_y^2) = \frac{(n + \frac{1}{2}eB)}{m^*}, \tag{15}$$

where the integer n runs up from $n=0$.

Historically, the effects of Eq. (15) gave the first direct evidence of quantum effects in electrical transport—the magnetotransport phenomena called the de Haas–van Alphen and Schubnikov–de Haas effects. The quantization repre-

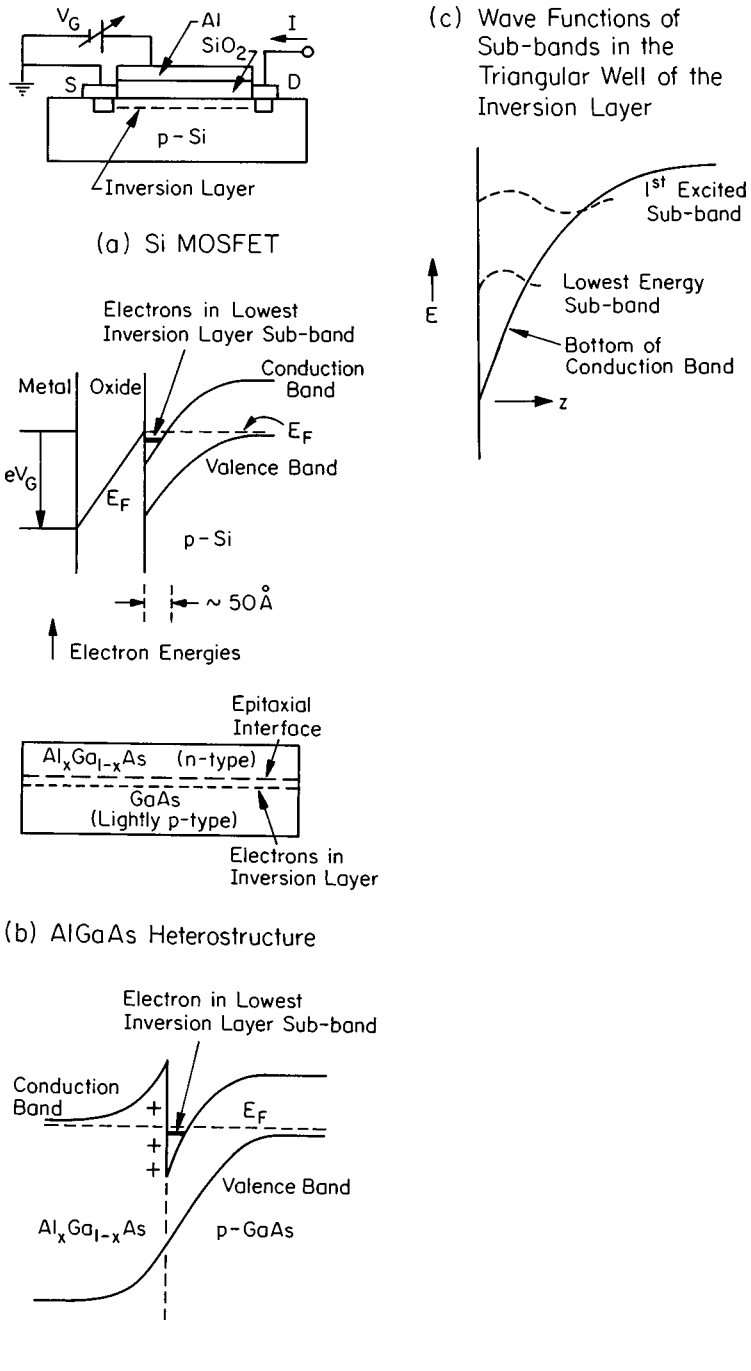

Fig. 6. Experimental realizations of systems with 2D electronic conduction. (a) Configuration of a typical Si MOSFET, and the resulting electron energy structure in the nominally *p*-type Si. Electron density in the 2D ''inversion layer'' immediately adjacent to the insulating SiO_2 layer is controlled by the gate voltage, V_G. (b) Configuration of a typical $Al_xGa_{1-x}As/GaAs$ heterostructure, and the resulting electron energy structure across the interface. Electron density in the inversion layer in the GaAs block is controlled by the $Al_xGa_{1-x}As$ band gap and doping levels. (c) Schematic of a triangular potential well formed in either of the structures, Si MOSFET or $Al_xGa_{1-x}As/GaAs$ heterojunction. The exact shape of the potential and of the wave functions for the various subband energies will, of course, depend on the characteristics of the particular interface.

sented by Eq. (15) is described in terms of the so-called ''Landau levels,'' which form a substructure in the band of one-electron, Bloch states in a chunk of metal.

1. Landau levels

In a 3D sample, the quantization of the conduction electron energy levels by the magnetic field into the cyclotron levels [Eq. (15)] shapes the spherical Fermi surface in **k** space into a series of coaxial cylinders, as shown in Fig. 7(b). In the 2D systems, the quantization takes a particularly clean form. Here, where k_z is always zero, the 3D coaxial cylinders collapse into concentric rings, with gaps in **k** space between the occupied states, as shown in Fig. 7(c). (Note that in 3D, there are no actual gaps in values of k^2, since values of k_z are unrestricted. Thus there will not be gaps in the *energy* distribution, whereas in 2D these gaps are evident.)

The separated ''Landau levels'' in the 2D system form the underpinning of the IQHE.

(I follow here a treatment given by Hook and Hall[26] which is particularly well-suited for the level of this article.)

With the Landau levels well separated, one wants to examine how the total number of conduction electron states distribute themselves among those levels. The number of states in k space in an interval dk, per unit area, in the absence of a magnetic field, is given by the expression

$$g(k)dk = \frac{k\ dk}{2\pi}. \tag{16}$$

The kinetic energy is $\hbar^2k^2/2m$. The density of states in energy per unit area becomes

$$g(\epsilon) = g(k)\frac{dk}{d\epsilon} = \frac{m^*}{2\pi\hbar^2}. \tag{17}$$

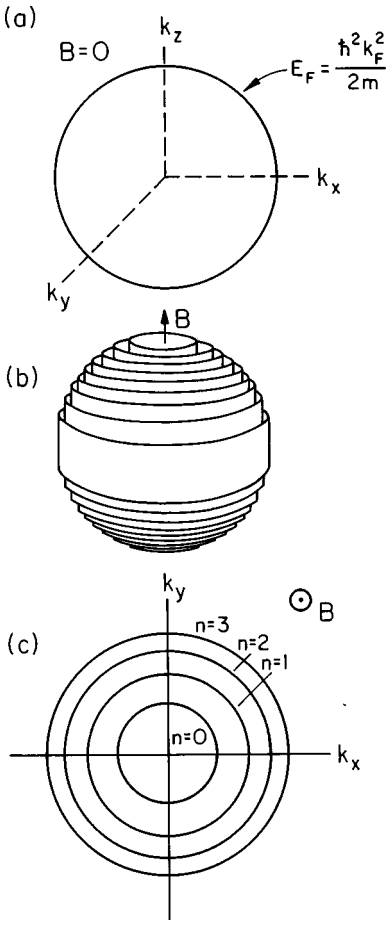

Fig. 7. States in k space occupied by conduction electrons, in three situations: (a) Free electron states in an isotropic, 3D metal, $B=0$. The electrons are uniformly distributed in **k** space within the Fermi sphere, up to the sharp (at $T=0$ K) Fermi surface. (b) Application of a large magnetic field in the z direction condenses the electron states in **k** space of (a) into cylinders concentric around the z axis. While there are regions of **k** vectors now excluded, there are no actual gaps in values of k^2, hence no gaps in kinetic energy. (c) In a 2D system, with **k** vectors constrained to the $x-y$ plane, the cylinders of (b) collapse into concentric rings, with gaps in kinetic energy between the rings.

When a magnetic field is added, the total energy of an electron can be written as

$$E=E_z+(n+1/2)\hbar\omega_c\pm\mu_B B. \tag{18}$$

In this expression, E_z represents the energy of the standing wave state in the z direction—the source of restriction of the motion to 2D. We'll assume that all electrons are accommodated in the lowest of these E_z subbands and will not further consider this energy. The second term is the cyclotron energy, with quantum number n, and the last term is the Zeeman energy of the electron.

Figure 8(a) and (b) suggests the subsequent story. All electron states over a range of energy $\hbar\omega_c$ collapse into each Landau level, with $\hbar^2k^2/2m=\hbar^2k_n^2/2m$. Because the zero-field density of energy states in 2D is independent of ϵ [see Eq. (17)], there will be the same number of energy states per unit area in each Landau level. Using the symbol N_L to designate this number, the average density of states with magnetic field on is $N_L/\hbar\omega_c$. Equating this to the last form given in Eq. (17), we have

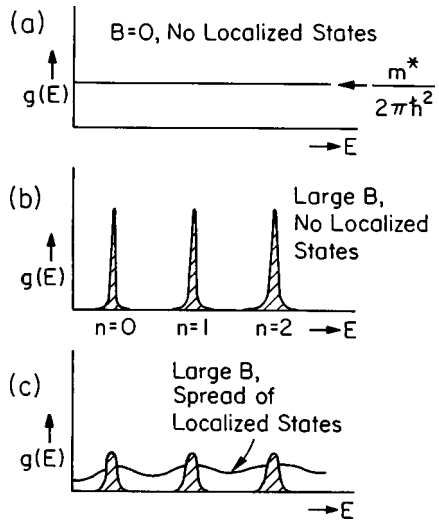

Fig. 8. Density of electron states/unit area/unit energy, $g(E)$, in the 2D system. (a) With $B=0$, the spinless density of states has the constant value $m^*/2\pi\hbar^2$. (b) With a large value of B, the states of (a) coalesce into the Landau levels, with some broadening due to such things as lifetime effects, sample impurities, etc. (c) If the sample has fluctuations in local binding potentials sufficient to generate large numbers of localized states with energies spread widely, the neat structure of (b) spreads out, with electron states sucked out of the Landau levels and spread over the full range of energy.

$$N_L=\frac{eB}{h}. \tag{19}$$

This expression counts the spinless states which appear in the sketches of Fig. 8(a) and (b). Each of these states is actually a doublet, to accommodate the two spin directions.

Side comment: One can write Eq. (19) in an alternative form,

$$\frac{n}{wL}=\frac{eB}{h}, \quad \text{or} \quad n=\frac{eBLw}{h}=\frac{e\Phi}{h},$$

where n is the total number of states/Landau level in the sample and Φ the total flux through the sample. We see that n measures the total flux in units of the flux quantum, h/e.

Remember that the value of the Fermi energy, E_F, is controlled by the electron density, n_A. Therefore, for an arbitrary value of n_A we expect E_F to fall somewhere within one of the Landau levels—these levels will, of course, be broadened from the sharpness of the simplest model by, for example, scattering of the circulating electrons.

2. Transport effects of magnetic field B

With the fields $\mathbf{E}=(E_x,0,0)$ and $\mathbf{B}=(0,0,B_z)$, the Drude drift velocity equation is

$$d\mathbf{v}_{D/dt}=-e/m^*[\mathbf{E}+(\mathbf{v}_D\times\mathbf{B})]-\mathbf{v}_D/\tau. \tag{20}$$

Treating Eq. (20) by components, restricting charge motion to the $x-y$ plane, gives

$$dv_{Dx}/dt=-e/m^*(E_x+v_{Dy}B_z)-v_{Dx}/\tau,$$

$$dv_{Dy}/dt=e/m^*(v_{Dx}B_z)-v_{Dy}/\tau=(\text{in steady state}),\ 0.$$

Consequently,

$$v_{Dx}/v_{Dy}=(m^*/eB_z)1/\tau=(\omega_c\tau)^{-1}\equiv\tan\phi_H, \tag{21}$$

where ϕ_H is often called the ''Hall angle.'' Note that as τ becomes longer (as it would normally do as the temperature of a material drops toward 0 K), $\mathbf{v}_D$ becomes more nearly perpendicular to **E**. However, in a typical Hall experiment, a nonzero value of E_y (the ''Hall field'') appears as a consequence of sample boundaries which block charge flow in the y direction.

The circulatory effects of the $\mathbf{v}\times\mathbf{B}$ term require a tensor description of σ and ρ. We write

$$\mathbf{j}=\sigma\cdot\mathbf{E} \quad \text{and} \quad \mathbf{E}=\rho\cdot\mathbf{j} \quad \text{where the tensor } (\rho)=(\sigma)^{-1}.$$

In the presence of a magnetic field $\mathbf{B}=(0,0,B_z)$, the conductivity tensor is given by

$$\sigma=\begin{pmatrix}\sigma_{xx}\sigma_{xy}\sigma_{xz}\\ \sigma_{yx}\sigma_{yy}\sigma_{yz}\\ \sigma_{zx}\sigma_{zy}\sigma_{zz}\end{pmatrix}$$

$$=\frac{n_A e^2\tau}{m^*}\begin{pmatrix}\dfrac{1}{1+\omega_c^2\tau^2} & \dfrac{-\omega_c\tau}{1+\omega_c^2\tau^2} & 0\\ \dfrac{\omega_c\tau}{1+\omega_c^2\tau^2} & \dfrac{1}{1+\omega_c^2\tau^2} & 0\\ 0 & 0 & 1\end{pmatrix}. \tag{22}$$

The resistivity tensor $\rho=\sigma^{-1}$ is found by inverting the conductivity tensor. After doing so, the individual elements can be usefully expressed in terms of the elements of σ,

$$\rho=\begin{pmatrix}\rho_{xx} & \rho_{xy}\\ \rho_{yx} & \rho_{yy}\end{pmatrix},$$

where

$$\rho_{xx}=\rho_{yy}=\frac{\sigma_{xx}}{\sigma_{xx}^2+\sigma_{yx}^2}, \quad \rho_{xy}=\frac{\sigma_{yx}}{\sigma_{xx}^2+\sigma_{yx}^2}. \tag{23a}$$

In the limit $\tau\to\infty$, σ_{xx} approaches zero, and $\sigma_{xy}\to-(1/\omega_c\tau)(n_A e^2\tau/m^*)$. Thus, in this limit,

$$\rho_{xy}=\begin{pmatrix}0 & \dfrac{1}{\sigma_{yx}}\\ -\dfrac{1}{\sigma_{yx}} & 0\end{pmatrix}$$

$$=\begin{pmatrix}0 & \dfrac{\omega_c\tau}{n_A e^2\tau/m^*}\\ -\dfrac{\omega_c\tau}{n_A e^2\tau/m^*} & 0\end{pmatrix}=\begin{pmatrix}0 & \dfrac{B}{n_A e}\\ -\dfrac{B}{n_A e} & 0\end{pmatrix}, \tag{23b}$$

where I have replaced ω_c with its equivalent, eB/m^*. Note that ρ_{xx} *also* approaches zero. The curious situation in which both σ_{xx} and ρ_{xx} approach zero is a consequence of the fact that if the scattering goes to zero, the electron drift velocity becomes orthogonal to the plane of **E** and **B**. To paraphrase Hook and Hall,[27] application of a longitudinal electric field E_x generates only a transverse current I_y, $(\sigma_{xx}=0)$—or: application of a longitudinal current generates only a transverse field, $E_y(\rho_{xx}=0)$.

The last form for the ρ tensor in Eq. (23) represents the classical Hall effect in the long τ regime. The ''Hall coefficient,'' $R_H=\rho_{xy}/B=1/n_A e$, measures the carrier concentration n_A, as we expect. (Remember that in 2D, ρ_{xy} is a resistance, measured in ohms.)

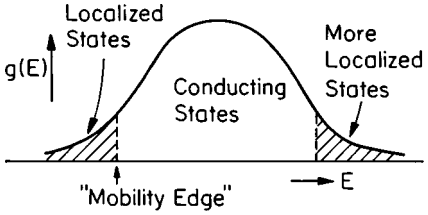

Fig. 9. A sketch of an electron energy band in a disordered material, with conducting and localized states, separated by the so-called ''mobility edge.''

C. Extended and localized electron states

Some of the ideas critical to our present model for the IQHE arise from the extensive experimental and theoretical studies of the localized electron states which occur in nominally conducting materials. The wave function of such a state has a modulating envelope which can be characterized by a multiplier of the form $\exp(-r/\xi)$, where r is the distance from the electron's potential center and ξ is the ''localization length.'' Because such localized states are central players in our present understanding of the IQHE, a short discussion of localized states is appropriate. Much of the previous study has been directed toward 3D systems, but the concepts and mechanisms are applicable to systems of lower dimensionality.

Appearance of the localized states may arise from one of several features of the material under study and, very importantly, the additional effects of a large magnetic field. Given here is a short list of sources of localization in materials at zero magnetic field.

(1) In perfectly periodic systems: An energy gap in the conduction band may open as a consequence of either strong correlation effects (the Mott–Hubbard metal–insulator transition) or temperature-induced crystal structure change (e.g., the material V_2O_3—Ref. 28).

(2) In structurally disordered systems: Localized states may appear as a consequence of a spread in local electron binding energies (''Anderson localization''), a spread generated by the structural disorder. Experimental identification of materials in which the localization arises from this feature *alone* is difficult, because electrons in most real systems have sufficient electron–electron interactions to invoke features of the Mott transition. Both qualitative reasoning[29] and numerical calculations[30] suggest that the densities of electron energy states when these localized states are present might follow a pattern suggested by Fig. 9.

(3) In nonstoichiometric materials, such as heavily doped semiconductors or a number of chemically mixed transition metal oxides (e.g., Na_xWO_3 or $La_{1-x}Sr_xVO_3$), the localized states can often be thought of as being generated by a failure of linkage from one impurity electron binding site to another. Said another way, the localization in such systems is a consequence of a variation in values of off-diagonal matrix elements of the Hamiltonian (i.e., transfer integrals) as opposed to a variation in diagonal matrix elements (i.e., energies of states) in systems described in paragraph (2) above. Percolation models are useful for these impurity systems.

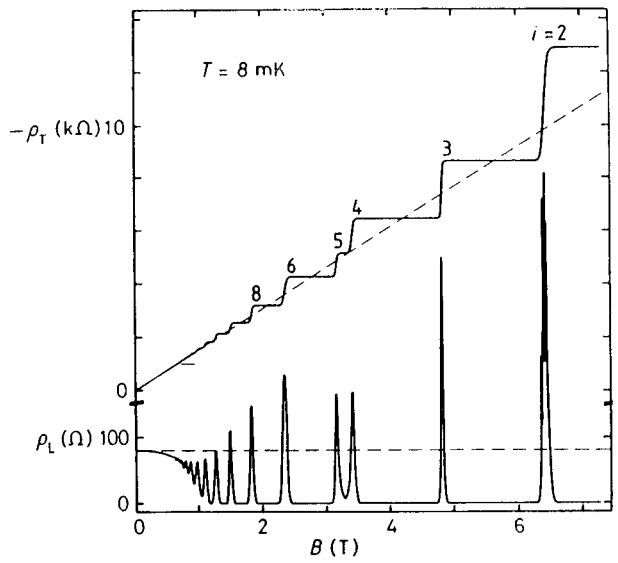

Fig. 10. Voltages V_H (measured by ρ_T) and V_x (measured by ρ_L) as a function of B_z for a GaAs–AlGaAs heterojunction at $T=8$ mK. The sharpness and width of plateaus, and the wide segments of B over which $V_x = \rho_L$ should be compared with matching data at $T=1.2$ K in Fig. 1(a). [Reprinted from K. von Klitzing, Physica B, C **126**, 242 (1984), with permission from Elsevier Science.]

The presence of a large magnetic field is expected to affect the balance between extended and localized electron states. Long-known is the so-called ''magnetic freeze-out'' effect, occasioned by a reduction of dimensions of electron orbitals by the $\mathbf{v}\times\mathbf{B}$ force.[31] A more complicated effect working toward *delocalization* arises from the effects of B in breaking the time-reversal symmetry of electron scattering events. The effects of this push toward delocalization are enhanced in 2D in comparison with 3D systems.

D. The Quantum Hall state

1. Observations

We're now prepared to return to a discussion of the remarkable features of Fig. 1(a)—plateaus in values of ρ_{xy} and zeroes in values of ρ_{xx}. (I will not include a discussion of the so-called ''fractional'' Quantum Hall Effect, in which additional plateaus appear at values of i which are ratios of integers. Theoretical models needed for such a treatment are well beyond the scope of this paper. Those models require explicit and thorough treatment of electron–electron interaction effects.[32])

Figures 1(a) and 10 show experimental data collected from high quality (i.e., long electron scattering lengths) samples of GaAs–GaAlAs at two different temperatures, 1.2 K for Fig. 1 and 8 mK for Fig. 10. In Fig. 1(a), V_H is a measure of ρ_{xy} and V_x is a measure of ρ_{xx}. These two figures characterize the dramatic facts of the IQHE with which we have to come to terms. (Comment: The original observations[1] of the IQHE were based on observations in Si MOSFETS. Most experiments since that time have used the GaAs system, in which substantially longer values of l_ϕ are achievable. However, the MOSFET observability is important because in the MOSFET one can control the occupancy of the Landau levels by changing *either* the magnitude of the magnetic field B *or* varying the conduction electron concentration by varying the gate voltage. This feature permits one to test the applicability of the Landau level model. B controls N_L [Eq. (19)] and n_A controls the energy position of E_F.)

(1) On the characteristic stairsteps of $\rho_{xy}=R_{xy}$, the values are $R_{xy}=25\,812.8\Omega/i$, where $i=$integer. This value has been reproduced to very high precision and with agreement by many investigators in different laboratories. In fact, the international measurement standards community has now shifted gears so that the reproduction of the value of the ohm is now *defined* in terms of measurement of R_{xy}.[33,34] Specifically,

$$1\Omega \equiv \frac{R_K}{25\,812.807},$$

where I have now adopted the symbol R_K, the ''von Klitzing constant,'' to represent the experimental value of (V_H/I_x) on the $i=1$ IQHE plateau at low temperature. [See Eq. (1).]

(2) Over the plateau width in ΔB, ρ_{xx} is essentially zero for values of T near 0 K—that is, the longitudinal voltage drop between measurement probes, V_x, vanishes.

(3) As the temperature is lowered, the plateaus become wider, the steps between them sharper, and the range in B over which ρ_{xx} differs from zero becomes narrower and narrower. At temperatures and values of B such that ρ_{xy} lies on one of the flat plateaus and the value of ρ_{xx} is zero, we characterize the system as being in the ''Quantum Hall state.''

To this point, I have ignored the effects of the Zeeman splitting, the last energy term in Eq. (18). In footnote 5 of Ref. 25, Eisenstein gives a clear, compact discussion of the effects of the Zeeman splitting on the observed plateau structure.

2. Interpretational model

In order to avoid getting lost in the weeds in discussion of a complicated, subtle and almost surely not yet completely understood phenomenon, it is useful to begin with a short list of the crucial legs upon which a credible explanation of the IQHE depends. (All of these effects were individually well-known before the discovery of the IQHE, but their significance in 2D systems became apparent only after that discovery.)

(1) Application of a strong magnetic field normal to the surface of a 2D electron system condenses the energy levels in a free electron system into discrete and well-separated groups—the 2D Landau levels.

(2) The motion of electrons in crossed **E** and **B** fields, with **B** perpendicular to the plane of the sample, is fundamentally anisotropic and has an intrinsic circulatory component. Most especially, as the electron scattering time, τ, becomes very long, the electron drift velocity becomes orthogonal to the plane of **E** and **B**.

(3) Any real conducting material, because of a certain degree of structural disorder (impurities, structural defects, etc.), is likely to have a certain number of localized electronic states as well as the primary delocalized (conducting) electron states. The localization properties are strongly affected by the presence of a large magnetic field. Energy levels associated with these localized electron states spread out from the well-defined Landau levels of the extended, transport state. They play a central role in supporting the sharp IQHE plateaus, as we shall see.

3. Filled Landau levels—the essential source of the quantization

Soon after the discovery of the IQHE, the experimentally observed plateaus in values of ρ_{xy} were identified with successive Landau levels in the sample. Our Eq. (19) recorded the fact that each successive Landau level has a total number of states per unit area $N_L = eB/h$. Thus, if we use the integer i to label the successive levels, the total number of electron states in i levels will be ieB/h. We postulate that each plateau of Fig. 1 is associated with the filling of one of the successive Landau levels.

There are n_A carriers to distribute among the i Landau levels. When the ith level is just filled, we have the relationship

$$n_A = iN_L = ieB/h. \tag{24}$$

Thus, at those special values of n_A and B that satisfy these equations and that place the value of E_F in the gap between two Landau levels, the ρ_{xy} tensor becomes

$$\rho_{xy} = \begin{pmatrix} 0 & \dfrac{h}{ie^2} \\ \dfrac{-h}{ie^2} & 0 \end{pmatrix}. \tag{25}$$

While this simple argument produces the values of ρ_{xy} seen in the IQHE, it is obviously *too* simple. It should be valid only at the special values of B at which a Landau level is exactly filled, whereas experimentally the plateaus in values of ρ_{xy} extend over a broad range of values of B. But the argument *does* suggest that we are on the right track by focusing on the quantization of the Landau levels as a central component in a full explanation.

4. Zero longitudinal resistivity

I noted in Sec. III B that as the value of scattering time τ becomes very large, both σ_{xx} and ρ_{xx} approach zero, even in the Drude–Sommerfeld model. In the Quantum Hall state the carrier scattering processes appear to be systematically inhibited, giving us $\tau \to \infty$ and a lossless current between the voltage-sampling electrodes which measure V_x. [Fig. 1(b)].

So far, so good, but the two central phenomena of the IQHE, $\rho_{xy} = R_{xy} = h/ie^2$ and $\rho_{xx} = R_{xx} = 0$, beg for further explanation. The argument that associates the plateau levels with filled Landau levels would appear to apply only for the particular values of n_A and B which exactly fill the level. At other values, the Fermi level would apparently lie within a particular, partially filled Landau level. But experimentally, the plateau extends over a substantial range of B for GaAs heterostructures, or of B or n_A for the Si MOSFETs. And in the case of zero value for ρ_{xx}, how is the inhibition of carrier scattering achieved? One answer for this double conundrum can be found in the special role of a certain concentration of localized electron states.

5. The localized states—capturing the Fermi level away from a Landau level

By now (18 years after the discovery of the IQHE) it appears certain that the existence of localized electron states in the 2D samples is crucial to observation of IQHE. The essence of the model is represented in Fig. 8(c), which sketches out a density of electron states that is plausible on the basis of earlier studies of localized states and is sufficient to describe the QHE observations.

Only mobile electrons, whose energy lies in the natural width of the Landau levels, participate in the Hall transport effects. If we construct a thought experiment in which the field B is slowly raised, we will stretch out the rungs of the Landau ladder, pulling them one by one up through the Fermi energy E_F, which is controlled by the total electron density n_A. With a sufficient number of localized states, E_F will fall in the range of these localized states over a broad swath of values of B. The Quantum Hall state is maintained by the electrons which lie in the extended states near the Landau level energy. The nonzero width of the transitions from one stairstep to another in Fig. 1(a) is associated with the small range of B over which E_F actually lies in the narrow range of the conducting states. The total inhibition of inelastic scattering of electrons in the conducting states signaled by the condition $\rho_{xx} = 0$ arises from the absence of nearby, empty energy states into which itinerant electrons can scatter.

It has been, and remains, very difficult to make and interpret sufficiently illuminating microscopic measurements to independently work out the energy level structure and spatial distribution of the localized states. But there are two kinds of experiments which provide evidence that the ''localized state model'' does provide an essential mechanism for keeping the Fermi level away from the Landau levels.

(1) Comparison of the data of Fig. 10 with those of Fig. 1(a) displays the strong temperature dependence of sharpness of the stairsteps. At 8 mK, the range of B over which the next Landau level is filled is much sharper than in the 1.2-K data of Fig. 1(a). This behavior is qualitatively consistent with the localized state model, since one expects electrons in some weakly bound localized states to be excited to conducting states at the higher temperature, compromising the sharpness of the peak of conducting Landau states.

(2) Direct experiments by *adding* sources of localized states: Furneaux and Reinecke[35] added extra Na^+ ions at the surface of a Si MOSFET 2D layer, and found the plateaus to be widened by this addition. This result is consistent with the idea that additional localized states would push the mobility edge up in energy so as to narrow the energy range of Landau level conducting states, thus narrowing the field span of the transition regions and broadening the plateaus.

At this point, a ''first-level'' model of the IQHE is complete. Section IV E addresses important but more intricate questions of why real measurements with real and sometimes messy probes on real samples produce the clean experimental data on ρ_{xx} and R_{xy}. A description of a possible mechanism by means of which electrons in the extended, Landau level states carry the longitudinal current while maintaining the $\rho_{xx} = 0$ condition is sketched out.

E. Microscopic nature of the Quantum Hall state

The localized state model as presented in its simple form in the preceding section leaves unanswered a variety of questions. Some of these questions immediately arise when we begin to investigate the microscopic nature of the Quantum Hall state—e.g., (1) why is the exact quantization in terms of h/e^2 so robust—a firm value seen by many observers in many different laboratories with many different samples? The exact spatial distribution of localized states or their dis-

tribution in energy does not seem critical—why not? What can be said about the nature of the imperfections which generate the localized states? (2) What are the actual patterns of electrical potential and current distribution in the 2D electron gas which support the Quantum Hall state? Relevant questions center around practical issues associated with real measurements on real samples.

These questions turn out to be deep and not easily answered. They have occupied the thoughts of many skilled observers and theoretical interpreters in the years since the first observations of the IQHE, and continue to do so. A full presentation of the best current understanding is beyond the scope of this paper (and beyond the competence of the author!). I can, however, sketch out some of the relevant ideas and models, and give the reader some connections to recent literature that describes ongoing research.

I believe it is fair to say that a sharp understanding of the sources of the localized states is a piece of unfinished business. Thus, that subject is not ripe for a discussion in a paper of this sort.

Investigations of the patterns of spatial distribution of electric potential and currents in the Quantum Hall state in experimental samples have been carried out by many experimentalists. These investigations continue, because of a number of nagging uncertainties. We'll briefly survey two of the central issues.

(a) Samples in the common ''Hall bar'' configuration[36] (with or without tabs for contact points) have finite values of the width. What is going on at the boundaries of the sample, at $y=\pm w/2$? [See Fig. 1(b).]

(b) What is the spatial distribution of the injected current which generates the Hall voltage V_H? Can we describe the current distribution in ways which are consistent with experimental observations *and* with the two key results—quantization of R_{xy} and $\rho_{xx}=0$? Are there specific requirements for making current injection and voltage measurement contacts?

1. Spatial distribution of longitudinal Hall current in the ''Hall bar'' configuration

Measuring the y dependence of the current density, $j_x(y)$, in samples occupying a Quantum Hall state and development of appropriate theoretical models to match the measurements have been important issues from the earliest days of the IQHE. A model postulating charge transport in quantum mechanical ''edge channels,'' conceptually similar to the quantum channels for transport in 1D systems, grew up shortly after the discovery of the IQHE. We'll outline the ideas behind this model, and briefly describe the current experimental state of affairs *vis-à-vis* observation of these currents, which reside very near the sample edge—within a distance from the sample edge roughly equal to the magnetic length, l_B. But, before doing so, it is important to clarify some electrical features of the 2D Hall systems which differ qualitatively from the more familiar 3D samples. These features produce a background complexity in the current distribution which require one to interpret experimental measurements of $j_x(y)$ carefully.

In the 3D Hall effect, the exterior surfaces of the sample transverse to the current direction behave in a rather benign fashion. A plausible model envisions a buildup of positive charges of uniform areal density at one face and negative charges at the other face. These charges generate a uniform electric field through the sample, just large enough to balance the Hall field $\mathbf{v}\times\mathbf{B}$.[37] It should be noted that this simple, intuitive model does not, in fact, quite correctly handle fields at the sample edges, even in the 3D case. But the 2D situation is intrinsically more complicated, never mind the specific quantum effects such as the edge channels to be discussed in Sec. IV E 2. In a 2D sample, a first-level model now starts with a *linear* charge density at the sample edge. The resulting electric field is now neither uniform within the 2D sample, nor even naturally limited to the sample material itself. It will, in general, spread into surrounding space. Figure 11 shows the electric potential resulting from this first-level model, in a plane formed by two long, parallel, line charges of opposite sign. The simple calculation leading to Fig. 11 is, of course, unrealistic in that the potential and electric field blow up as one approaches the line charges. It is clear that the unbalanced charge distribution at either edge will spread into the material, reducing the sharpness of the potential (and field) rise.

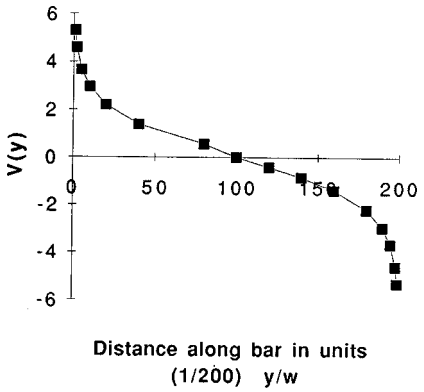

Fig. 11. A plot of potential $V(y)$ in a plane between two line charges of opposite sign parallel to the x axis. $V(y)$ is the sum of the two appropriate logarithmic expressions (see the text). The plot is cut off before it reaches either edge of the plane—in this simple model, $V(y)$ blows up at either edge. Scales for values of both $V(y)$ and y are in arbitrary units.

A more serious calculation of a self-consistent value of potential, $V(y)$, across a sample has been carried out by MacDonald, Rice, and Brinkman.[38] To quote from their abstract, ''Using a Hartree approximation we derive a self-consistent equation which describes the charge, current and Hall voltage $[V(y)]$ distributions in a two-dimensional electron gas with filled Landau levels'' (i.e., a sample in the Quantum Hall state). The general shape of their result for $V(y)$ is, in fact, quite similar to that of Fig. 11.

I turn now to experimental measurement of $V(y)$. In order to obviate perturbative effects generated by the attachment of voltage probes at various positions across the sample, Fontein *et al.*[39] probed the value of $V(y)$ with a scheme which uses a fine laser beam and the Pockels effect. Figure 12, taken from Ref. 6, shows the central outcome of their experiment as well as the results of a model calculation which is a slight simplification of the approach of MacDonald *et al.*[38]

Having determined the potential, the longitudinal current distribution $j_x(y)$ can be obtained from the equation

$$j_x(y)=\frac{n_A e}{B}\frac{\partial V_y}{\partial y}. \tag{26}$$

(The source of this equation is described in Appendix A.) Application of Eq. (26) to the shape of $V(y)$ shown in Fig.

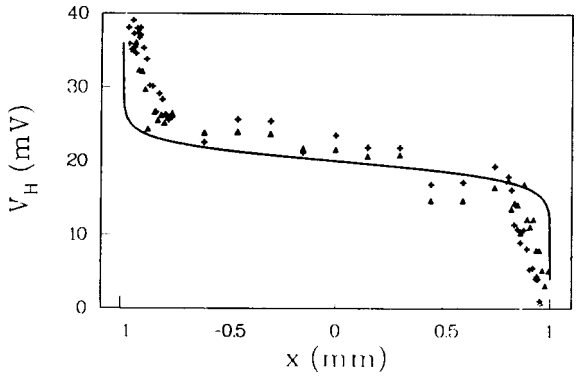

Fig. 12. Measurements and calculations of a Hall potential $V_H(y)$ induced by passing a longitudinal current, $I_x = 5\ \mu$A, through a 2D Hall effect sample. The data points show measurements of $V_H(y)$ that were made by Fontein *et al.* (Ref. 40) by observing the birefringence of GaAs induced by the electric field, $E_y = -dV(y)/dy$. The spatial resolution of the measurement was given as 70 μm. Their scheme is one of several which have been introduced to avoid the field perturbations induced by electrical contacts. The solid curve gives a calculation based on the work of MacDonald *et al.* (Ref. 39). The figure is taken from Ref. 6, reproduced by permission of Academic Press, Inc.

12 leads to a current distribution which is strongly peaked near the sample edges—a result which complicates investigations of the postulated edge currents to be discussed in the following paragraphs.

Using Eq. (26) to determine values of j_x from Fig. 12, Fontein *et al.* found that two-thirds of the total current was carried in the steep regions of V_y near the sample boundaries and one-third in the interior region.

Fontein *et al.* give the spatial resolution of the measurements of Fig. 12 as 70 μm. This length interval is too large to permit use of these results to test the applicability of the edge channel model described in Sec. IV E 2. However, these results describe an overall current pattern within which models appropriate to measurements with finer resolution must fit.

In preparation for the following discussion of edge currents, we should note, however, that the characteristic length scale over which substantial changes in $V(y)$ occur is *much* larger than the magnetic length, l_B, which turns out to characterize the depth within which one expects the edge currents to flow. MacDonald *et al.* explicitly eschewed consideration of the edge currents in their paper.

2. Phenomena at sample edges—transport in ''edge channels''

Figure 13 gives a model of a Hall bar with appropriate contacts for injecting current and measuring relevant voltages. First suppose that no net current I_x is being injected. The labeled ''edge currents'' flow as a consequence of the existence of the edges which interrupt the cyclotron orbits. These currents represent part of the diamagnetic circulation set up in the course of turning on the field B. In a semiclassical picture, they are formed by the so-called ''skipping orbits.''[40] We expect these currents to flow near the sample edge in a layer of thickness equal to roughly the radius of a cyclotron orbit. (Table I gives a value of about 10 nm=100 Å for the orbit radius in the lowest Landau level at $B = 10$ T, a typical value for high-field IQHE investigations.)

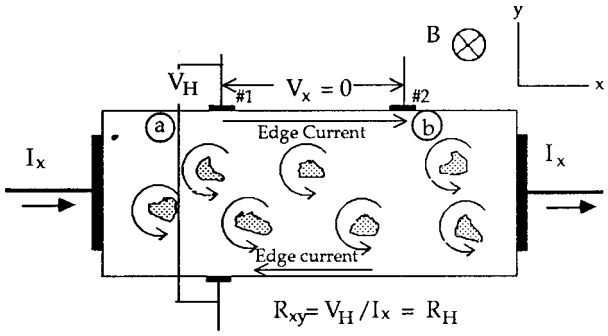

Fig. 13. A schematic rendition of a Hall effect 2D sample, with notation matching that of Fig. 1(b). We focus now on patterns of charge flow within the sample, with the stipulation that B is sufficiently large that a cyclotron orbit radius is very much smaller than the sample width, w. (Easily satisfied in large fields—see Table I.) The ''Edge currents'' derive from the so-called ''skipping orbits,'' occasioned by specular reflection of cyclotron motion at the sample edges. The cross-hatched regions represent patches of sample occupied by electrons in localized states, with encircling currents derived from local skipping orbits.

To investigate the energetics of the situation near the sample boundaries, we need the energy diagram of Fig. 14. At the two edges of the sample, where $y = \pm w/2$, the Landau level energies turn upwards in response to the confining potential. The edge currents are populated by electrons at the Fermi energy in these turned-up Landau levels. Figure 14 is set up on the assumption that particular values of n_A and **B** have set the Fermi level E_F so that only the first two bulk Landau levels are occupied. The edge current will then be formed from electrons in both of these levels. The terminology ''edge channels'' has been introduced to describe the contributions to the edge current from the wave functions of different Landau levels. In the case chosen for Fig. 14, two quantum ''channels'' are occupied. The term ''channels'' is used in the same sense as in our earlier description of quantization of 1D conductance. That is, electrons in each quantum state established by the confinement can separately con-

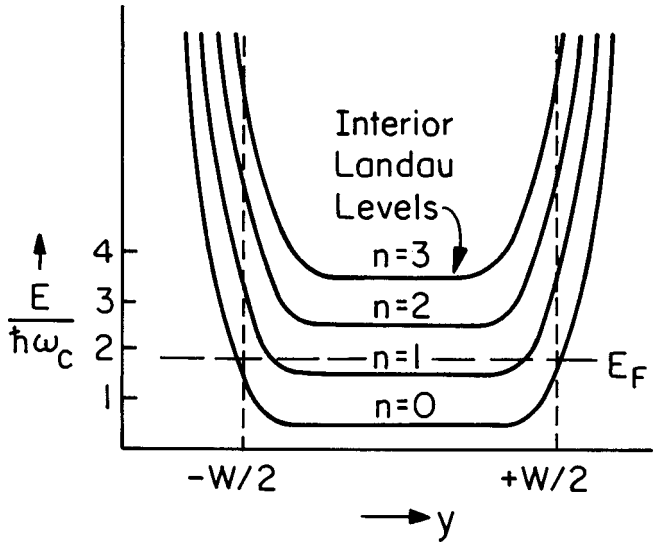

Fig. 14. A model of ''what happens to Landau energy levels at sample boundaries.'' This sketch envisions a rectangular well, with walls at the sample edges, $y = \pm w/2$. With the value of the Fermi energy, E_F, as shown, two Landau levels pass through E_F near the sample edges, giving rise to two ''edge channels.''

tribute to the overall current, forming a ''channel.'' In the discussion of Sec. III, the confinement was engineered by voltage gates. For the IQHE, the edge channels are set up by the sample boundaries that are responsible for the confining potential of Fig. 14.

Note that the electrons forming the edge channels lie at the Fermi energy, with nearby, unoccupied energy states available. Thus, these electrons are available to carry current under the impetus of an applied electric field.

One model for the IQHE has been developed in which properties of these edge currents combine with the existence of localized states to establish the fundamental quantum relation for the Hall resistance, $R_{xy}=h/ie^2$, and the accompanying condition, $\rho_{xx}=0$. This picture began with an ingenious argument introduced by Laughlin[41] and elaborated and extended by Halperin.[42] Another version of the argument is given by Kittel.[43]

Büttiker[44] has argued that the existence of the Quantum Hall state can be understood in terms of the special properties of current injected into these edge channels by the external current source. Büttiker gives a particularly thorough and measurement-oriented picture of how the Quantum Hall state develops in macroscopic samples with real contact probes.

It is not possible to do Büttiker's treatment justice in a short space in this paper. But the two key IQHE key results [$R_{xy}=h/ie^2$, and $\rho_{xx}=0$] emerge, provided that two conditions are maintained: (1) The probes #1 and #2 in Fig. 13 which measure V_x must be sufficiently distant from the current injection and extraction contacts that a well-defined chemical potential (i.e., thermodynamic equilibrium) is established in the regions labeled *a* and *b*. (2) The magnetic field *B* must be sufficiently large that the sample width *w* is much greater than the magnetic length l_B. In Büttiker's model, the quantum number *i* is given directly by the number of edge channels which are occupied at the given values of n_A and *B*. (As an example: For the sketch of Fig. 13, with two edge channels occupied by electrons with two spin states, we would have the Quantum Hall state with $R_{xy}=h/4e^2$.) Implicit in Büttiker's treatment is his central physical argument, that the particular form of electron response to the large magnetic field—i.e., the skipping orbit structure shown in Fig. 13—inhibits electron scattering across the sample from left-going to right-going edge currents. Absence of this cross-sample scattering is sufficient to give the ''perfect conductor'' behavior of the edge path between probes #1 and #2, even though these electrons in the edge channels *are* near the Fermi level and are, in principle, subject to scattering. We note that the existence of sample boundaries has required an elaboration of the earlier argument, that for values of E_F between Landau levels, no scattering could occur.

3. Experimental investigations of the edge channel model

In the complicated but elegant picture developed by Büttiker, the longitudinal current is carried entirely in the edge channels. However, his treatment is essentially a ''small current'' model, and does not really exclude the possibility that some current might also be carried across the full width of the sample. Experimental exploration of this issue by a great variety of experimental schemes has been extensive. A number of these experiments[39,45,46] demonstrate rather conclusively that (1) well-defined edge currents do exist, but that (2) current can also be carried throughout the width of the sample. Reference 45 gives an extensive list of other experiments whose results bear upon the question of current distribution.

The experiments described by Jeanneret *et al.*[46] employed a Corbino-disc sample geometry. From their results, the authors draw the conclusion that while edge currents in the form suggested in Fig. 13 certainly exist, currents may also flow without dissipation in the bulk of a sample which is in the Quantum Hall state. A similar conclusion is given by Beenakker and van Houten (Ref. 6, p. 177). But one should note that the radial bulk currents measured by Jeanneret *et al.* represent the analog of a transient current j_y in the Hall bar configuration. Thus, while their results are significant, they do not bear immediately on the issue of edge current versus bulk current in Hall bar measurements. They do, however, highlight the possibility that more experiments with samples in the Corbino geometry may yield important information to supplement the Hall bar measurements. (See Appendix B for a brief discussion of the Corbino disc geometry and the Jeanneret *et al.* results.)

Is there a consistent picture which can accommodate both the edge channel model and experimental results of the sort displayed in Fig. 12? In the Bütikker picture, lossless current carried in edge channels maintains an equipotential along the sample edges, as measured by V_x [Fig. 1(b).] These edge currents are composed of electrons at the Fermi level. The suppression of large angle scattering from states at one edge into either states at the opposite edge or into interior states is shown by Büttiker to give both conditions, $\rho_{xx}=0$ and the quantization of R_{xy}.

In the interior regions far from the edges, electrons in extended states within Landau levels below E_F can carry current, but dissipative scattering is inhibited by the unavailability of nearby energy states. (Remember that this situation is familiar in ordinary metallic conduction. Only electrons which at the moment occupy states within an energy *kT* of the Fermi energy E_F are subject to scattering, but the full electron distribution moves along at the drift velocity.)

It seems possible that the existence of local variations of potential or of charge density n_A in the interior of a sample can accommodate a melding of the Laughlin–Halperin–Büttiker model with the experimental realities of the sort exhibited in Fig. 12.[47] For example, nonconducting islands (host areas for localized states) in the interior of the sample, suggested in the sketch of Fig. 13, may promote a local equivalent of edge channels. The experiments of van Haren *et al.*,[45] in which internal energy shifts are generated by adding a transverse gradient in local values of n_A, show how internal quantum channels can be formed. Recent experiments by Tessmer *et al.*[48] probe local values of n_A by means of a capacitive measure of subsurface charge accumulation, and show how these values may vary as a consequence of some local properties of the 2D electron system.

While a 1993 theoretical paper by D. B. Chklovskii and P. A. Lee[49] is directed primarily toward analysis of transport phenomena observed when **B** lies in the transition ranges between IQHE plateaus, the model described in its introductory section gives clues toward a satisfactory picture of the effects of disorder when the system does fall in a plateau region. That introductory section points toward one source of disorder specific to the GaAs heterostructure samples, namely, the effects of inhomogeneities in the spatial distribution of the ionized donors in the AlGaAs layer (see Fig. 6).

Such inhomogeneities will result in variations in the local value of n_A, the electron concentration in the GaAs inversion layer. These variations can, in turn, lead to a mixed state, with a Quantum Hall state threading through other regions. A complete picture of the Quantum Hall state in real samples may demand full knowledge about the interior, disordered structure of experimental samples, knowledge not yet available.

A different and useful perspective on the overall problem of the current distribution, from a phenomenological point of view, has been developed by Cage and Lavine.[50] As in Sec. IV C of this paper, Cage and Lavine focus on consideration of the potential distribution function, $V(y)$. They consider a potential distribution function which is a combination of the ''confining potential'' (as shown in Fig. 14 of this paper) and a ''charge-redistribution potential'' (of form similar to the solid curve of Fig. 12). Again, the current distribution $j_x(y)$ can be obtained with the use of Eq. (26). Their results for $V(y)$ and $j_x(y)$ reinforce the conclusions reached in Ref. 39.

In summary, the difficult issues of establishing the actual functional form of $j_x(y)$ in samples residing in the Quantum Hall state, and the relationship of this form to such matters as (a) the spatial nature of the localized states within a sample or (b) the magnitude of the total current I_x remain matters of unfinished business.

Not surprisingly, there is a maximum value of the longitudinal current density j_x beyond which the IQHE is destroyed. The specific value will, of course, depend on various conditions of sample and experiments. As one example, Ebert *et al.*[51] found a breakdown in the IQHE in their particular sample above a value $j_x \cong 1.0$ A/m at $B=6$ T. (Such a value of current density corresponds to a current of about 100 μA in a sample with width $w=100\,\mu$m.)

F. State of the theoretical model

To summarize: The picture I have sketched out—quantization in Landau levels, with level filling maintained by capturing the Fermi level in a regime of localized states, and conditions on ρ_{xx} and R_{xy} maintained by the particular quantum dynamics of electrons in a very large magnetic field—appears to provide a coherent and rather complete model with which to describe the observed phenomena of the IQHE. In spite of this success, however, a fully developed and predictive microscopic theory, with supporting experimental measurements, has remained elusive. Eighteen years later, the Quantum Hall state remains an object of intensive study!

V. A BRIEF TREATMENT OF QUANTUM INTERFERENCE EFFECTS (REF. 52)

A. Coherent backscattering and ''weak localization''

An early experimental example of visible effects of electron quantum interference was the observation, as the temperature was decreasing near $T=0$ K, of a small increase in resistance of a material in which that resistance is controlled by elastic scattering from impurities or other crystalline defects. In a sequence of theoretical papers noted in a nice 1984 tutorial and review paper by Bergmann,[53] it was proposed that this resistance increase results from a quantum electron self-interference effect which accompanies elastic scattering of electrons by impurities or other structural defects. The

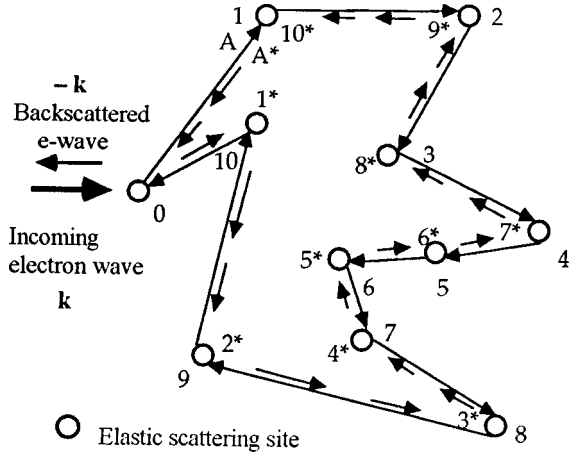

Fig. 15. A sketch of a pair of electron paths a la Feynman which contribute to coherent backscattering of electrons at low temperature, where the phase-scrambling effects of inelastic scattering are fading away. In a path-integral type calculation of the evolution of an electron wave function following a scattering event at the origin 0, one might find a clockwise path in the course of which the electron experiences ten elastic scattering, phase-preserving events and returns to 0. Also appearing will be a time-reversed (counterclockwise) path of the same shape in which the total phase accumulation matches that of the clockwise path. The constructive interference of the two paths, upon return to the origin 0, enhances the backscattering effect at low temperatures. The consequence is a small increase in measured resistance of the sample. (Idea for sketch taken from Fig. 2.5 of Ref. 53.)

effect is graphically described as ''coherent backscattering'' (CBS). Figure 15 conveys the idea. The clockwise path labeled A represents a possible trajectory (in the Feynman path-integral sense) in which a series of elastic scattering events takes the electron back to its starting point. In the Feynman picture, for every phase-preserving path A, there is a companion time-reversed path A* with exactly the same set of phase shifts, taken in inverse sequence. When all possible paths are summed, the pair A and A* will give constructive interference which constitutes a nonzero contribution to backscattering from the array of elastic scattering centers. Key to the development of the model suggested in Fig. 15 was the realization that while elastic scattering inhibits the free motion of the electron in the classical sense, it does *not* destroy the QM phase coherence of the electron wave function. In other words, while there may be a phase *shift* associated with the scattering, that shift would be the same for successive encounters of the particular scattering center by electrons of the same **k** vector. Said another way: If a monochromatic beam of electrons is projected through an array of elastic scattering centers, an interference pattern would be seen on a surrounding screen. We emphasize that the two paths sketched in Fig. 15 are *not* those of two electrons, but rather two symbolic paths of wave function development, in the Feynman path-integral framework.

This enhancement of backscattering has been called ''weak localization.'' A more descriptive term would probably be ''incipient localization.'' I note that the model suggested by Fig. 15, used by Bergman, turns out to be valid only in the regime in which $k_F l_{\rm el} \gg 1$. This condition itself signals that we remain in the conducting regime, well above the Ioffe–Regel limit alluded to in Table II.

Confirmation of the CBS model for the anomalous resistance increase came from observations that application of a magnetic field (to produce a *different* set of phase shifts in

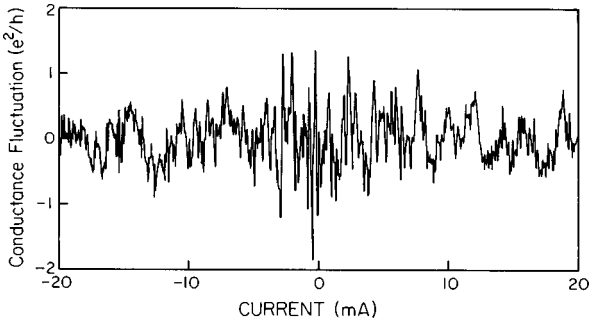

Fig. 16. Fluctuations in conductance of a 0.6-mm length of antimony wire, as a function of current through the wire. Note that the departures from ohmic behavior (i.e., G independent of I) are ''random'' in the sense that the patterns for positive and negative currents are not connected by any obvious symmetry. [Reprinted from ''Quantum Interference Fluctuations in Disordered Metals,'' by Richard A. Webb and Sean Washburn, Phys. Today **41**, 46–53 (December 1988), with permission of the American Institute of Physics.]

the clockwise and counterclockwise paths of Fig. 15) depresses the resistance increase by destroying the coherence which generates the CBS effect. Curiously enough, the resistance rise could also be depressed in some cases by *raising* the temperature—as the temperature rises, the electron phase memory time τ_ϕ is decreased, thus diminishing the strength of the CBS by interrupting the phase-preserving paths of Fig. 15. While the effects of CBS can be seen in bulk, 3D samples, the effects are more pronounced in 2D, where the restriction to a plane of Feynman paths of the sort sketched out in Fig. 15 strengthens the backscattering.

The quantum electron CBS has its precise analog in the coherent backscattering of light in an irregular optical medium, as recently described by Corey, Kissner, and Saulnier in this Journal.[54] Optical analogues of many of the other electron quantum interference phenomena (and vice versa) exist.[55]

B. Conductance fluctuations—a sample-specific quantum interference effect

A final item in our list of striking quantum interference effects is the phenomenon which has been termed ''Universal'' Conductance Fluctuations. The term ''universal'' means that it is a phenomenon seen in all 1D or 2D mesoscopic samples with substantial disorder, provided that the phase conserving length l_ϕ is much greater than the distance between voltage measurement probes. Figure 16 displays differential conductance measurements made by Webb, Washburn, and Umbach,[56] as a function of current, for a 0.6 mm length of Sb ''wire.'' The sample dimensions transverse to current flow were 0.08 μm by 0.1 μm. The sample temperature was 10 mK, in a magnetic field of 3 T. Note that the pattern of fluctuations is not symmetrical about zero current. The fluctuations do not represent the usual *time-dependent* noise sources. They are dependent on the *voltage difference* ΔV applied between sample ends.

These variations in G can be generated by either changing the electrochemical potential across the sample, as in Fig. 16, or in a MOSFET by varying the gate voltage, by changing the value of an applied magnetic field, or by altering the distribution of inelastic scattering centers. It is found that whatever the scheme used to generate δG, the fluctuations in G, the condition

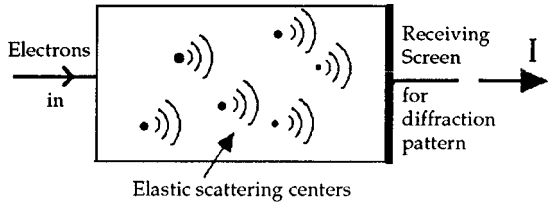

Fig. 17. Sketch to suggest how elastic scattering from a particular impurity configuration leads to a particular quantum interference pattern, and, hence, to a particular pattern of conductance fluctuations, such as shown in Fig. 16.

$$\sqrt{(\delta G)^2} \approx e^2/h$$

is maintained.

A great variety of experiments and a full theory by Lee, Stone, and Fukuyama[57] make it clear that these fluctuations arise from quantum interference patterns whose exact form changes when electron paths are altered by changing total current, magnetic field, or Fermi level. Figure 17 suggests what is going on. The form of an electron wave front which traverses the sample and reaches a measurement probe is determined by the configuration of the set of diffracting objects (i.e., elastic scattering centers) between current injection and measurement. Varying any parameter which alters the electron flow pattern among the scattering centers (e.g., an applied magnetic field) will change the output waveform and, hence, change the total current. This description would suggest that changing the concentration or configuration of elastic scattering centers would generate a different pattern of fluctuations. Various indirect experiments show that surprising conclusion to be exactly true! While repeating a given experiment on a given sample will always generate the same pattern, that particular pattern is native to the that particular conducting sample, provided the scattering center distribution is not changed.

I emphasize that these variations in G are *not* ascribable to various known sources of *time-dependent* electrical noise—e.g., Johnson noise, shot noise, $1/f$ noise. The magnitude is much larger than, e.g., the Johnson noise, at the low temperatures which are required to keep l_ϕ sufficiently long. Moreover, the observed repeatability of a given pattern for a given sample excludes these random noise sources.

VI. SUMMARY

By reducing one or two dimensions of a 3D conducting sample to lengths comparable to the Fermi wavelength, a number of electron quantum wave effects are made manifest. Each of them stems from some combination of several basic quantum-mechanical phenomena.

Quantized conductance in 1D systems: The stairstep values of conductance G stem from successive occupancy of the various current channels which are associated with the quantum levels determined by the width of a conducting pathway (''waveguide modes''). Samples are 1D in the sense that the quantum standing wave patterns direct charge flow along a single dimension.

Integral Quantum Hall Effect: The discrete Landau levels formed in a 2D sample are fundamentally responsible for the plateaus seen in the Hall resistance $V_H = IR_{xy}$. But key to a full description of the pattern of current flow and the vanishing of longitudinal resistance ρ_{xx} in a Hall experiment are (1) the role of localized states for many electrons, and, for the

Hall bar configuration, (2) the effect of sample edges, which push Landau levels through the Fermi energy and generate the quantized edge currents important to stability of the Quantum Hall state.

Quantum interference effects (also seen in 3D in muted form): For samples with dimensions small compared to the phase coherence length l_ϕ but large compared to the inelastic length, $l_{\rm el}$, a variety of effects which arise from electron interference patterns within the bulk materials of mesoscopic dimensions can be found and studied. These effects (coherent backscattering, quantum interference patterns, universal conductance fluctuations) can be understood in terms of a model in which the key event is an elastic scattering, with retained phase memory, of an electron by an impurity or other defect in the lattice of the conductor.

ACKNOWLEDGMENTS

I am particularly indebted to R. H. Silsbee for a series of illuminating discussions concerning various topics covered in this paper, and to D. C. Ralph for a number of useful comments. A number of changes resulted from the careful reading of the manuscript by two referees.

APPENDIX A: RELATIONSHIP BETWEEN $j_x(y)$ AND V_y IN THE HALL BAR CONFIGURATION

In modeling the actual electron motion in an externally injected current I_x under the effects of a large magnetic field B_z the concept of ''guiding center drift'' (of the cyclotron orbit center)[58] has been introduced. The drift velocity of this guiding center motion can be described by the equation

$$\mathbf{v}_{\rm drift}(x,y,z)=\frac{1}{B^2}\boldsymbol{\nabla} V\times\mathbf{B}.$$

Hence,

$$v_x=\frac{1}{B^2}\frac{\partial V_y}{\partial y}B_z,$$

and, thus, the current density $j_x(y)$ is given by

$$j_x(y)=n_A e v_x=\frac{n_A e}{B}\frac{\partial V_y}{\partial y}.$$

APPENDIX B: THE CORBINO DISC CONFIGURATION

Figure 18 shows the basic idea of the physical arrangement introduced by O. M. Corbino[59] in the early 20th century to permit measurements of the Hall effect in circular, thin puddles of liquid conductor. In his initial arrangement, current was injected at the center of a disc, and collected in a circumferential, bounding circular ring. With this arrangement, Hall current flows azimuthally around the disc (or ring) in response to the $\mathbf{v}\times\mathbf{B}$ force.

With ac excitation, the Corbino configuration avoids questions associated with unknown effects of current injection or voltage measurement contacts. Two schemes, inverses of one another, are possible. (1) Driving an ac radial current density, i_r, generates an azimuthal, alternating Hall current. A search coil with plane parallel to the disc will pick up the alternating B field arising from the Hall current. (2) Application of an alternating field parallel to the main, static field B_0 will generate an alternating azimuthal current by Faraday's law. Actions of B_0 on this azimuthal current will, in turn, generate an alternating radial Hall current, i_r.

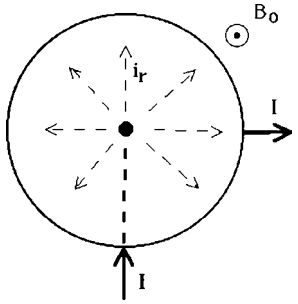

Fig. 18. Sketch of the Corbino disc geometry. In practice, most modern experiments, such as those of Ref. 46, use ac excitation, either by (a) applying i_r as an ac current, then sensing the resulting azimuthal Hall current with a pickup coil, or by (b) adding an ac component to the perpendicular magnetic field B_0, using Faraday's law to generate an ac azimuthal current in the disc. In this case, i_r appears as an alternating Hall current.

The scheme labeled (2) in the preceding paragraph is an experimental realization of the *gedanken* experiment introduced by Halperin, which he used to illuminate the source of the basic quantization, $V_r=I_\varphi ih/e^2$. Jeanneret *et al.* employed an arrangement of this sort. They find the alternating radial current to be lossless. There is no obvious place for edge channels to flow in the radial direction, and they conclude that the existence of edge currents is not required in order to give the lossless currents characteristic of the IQHE. (This alternating radial current is associated with the electron transfer from inner edge to outer edge of the Corbino sample which is featured in the Halperin version of the Laughlin argument.)

[1]K. von Klitzing, G. Dorda, and M. Pepper, ''New Method for High-Accuracy Determination of the Fine-Structure Constant Based on Quantized Hall Resistance,'' Phys. Rev. Lett. **45**, 494–497 (1980).

[2]B. J. van Wees, H. van Houten, C. W. J. Beenakker, J. G. Williamson, L. P. Kouwenhoven, D. van der Marel, and C. T. Foxon, ''Quantized conductance of point contacts in a two-dimensional electron gas,'' Phys. Rev. Lett. **60**, 848–851 (1988).

[3]D. A. Wharam, T. J. Thornton, R. Newbury, M. Pepper, H. Ahmed, J. E. F. Frost, D. G. Hasko, D. C. Peacock, D. A. Ritchie, and G. A. C. Jones, ''One-dimensional transport and the quantisation of ballistic resistance,'' J. Phys. C **21**, L209–L214 (1988).

[4]C. Kittel, *Introduction to Solid State Physics* (Wiley, New York, 1996), 7th ed.

[5]Most topics contained in this paper are covered in detail in one of two monographs—*The Quantum Hall Effect*, edited by Richard E. Prange and Steven M. Girvin (Springer-Verlag, New York, 1990), 2nd ed.; M. Janßen, O. Viehweger, U. Fastenrath, and J. Hajdu, *Introduction to the Theory of the Integer Quantum Hall Effect* (VCH, Weinheim, 1994); or in the extensive article listed as Ref. 6.

[6]C. W. J. Beenakker and H. van Houten, ''Quantum Transport in Semiconductor Nanostructures,'' in *Solid State Physics: Advances in Research and Applications*, Vol. 44, edited by Henry Ehrenreich and David Turnbull (Academic, San Diego, 1991).

[7]C. T. Van Degrift and M. E. Cage, ''Resource Letter QHE-1: The integral and fractional Quantum Hall effects,'' Am. J. Phys. **58**, 109–123 (1990).

[8]Richard A. Webb and Sean Washburn, ''Quantum interference fluctuations in disordered metals,'' Phys. Today **41** (12), 46–55 (1988).

[9]Paul L. McEuen, ''Artificial Atoms: New Boxes for Electrons,'' Science **278**, 1729–1730 (1997). This short article serves as an introduction to several more extensive papers in the same issue of Science (pp. 1784–1794) which focus on energy levels in quantum dot systems.

[10]L. P. Kouwenhoven, C. M. Marcus, P. L. McEuen, S. Tarucha, R. M. Westervelt, and N. W. Wingreen, ''Electron Transport in Quantum Dots,''

in *Mesoscopic Electron Transport*, edited by L. L. Sohn, L. P. Kouwenhoven, and G. Schon (Kluwer, Dordrecht, 1997), p. 105.

[11]For those readers who might be motivated to explore in depth the detailed dynamics of electron motion in the presence of electric and magnetic fields as pictured in the Drude–Sommerfeld model, an illuminating resource is the pair of interactive computer simulation programs entitled ''DRUDE'' and ''SOMMERFELD'' which are contained in a guidebook and CD by Robert H. Silsbee and Jörg Dräger, *Simulations for Solid State Physics* (Cambridge U.P., Cambridge, 1997). The fortuitous two-dimensional limitation of the computer screen turns out to favor examples and exercises which are played out in 2D and, thus, directly applicable to the systems of interest in this paper.

[12]For those readers who wish to study in detail the nature of electron transport in the quantum realm, a thorough treatment is given on pp. 1–80 in the treatise *Quantum Transport in Semiconductor Nanostructures*, by C. W. J. Beenakker and H. van Houten, listed in Ref. 6.

[13]See the article ''Quantum Point Contacts,'' by Henk van Houten and Carlo Beenakker, Phys. Today **49** (7), 22–27 (1996) for a treatment which parallels this section.

[14]R. M. Landauer, ''Spatial variation of currents and fields due to localized scatterers in metallic conduction,'' IBM J. Res. Dev. **1**, 223–231 (1957); **32**, 306–316 (1988).

[15]A good discussion of the use of this wave transmission/reflection model to treat electrical conductance is given by Yoseph Imry in an article entitled ''Physics of Mesoscopic Systems,'' in the review volume *Directions in Condensed Matter Physics*, edited by G. Grinstein and G. Mazenko (World Scientific, Singapore, 1986).

[16]Reference 6, pp. 111–112.

[17]A. Yacoby, H. L. Stormer, Ned S. Wingreen, L. N. Pfeiffer, K. W. Baldwin, and K. W. West, ''Nonuniversal quantum fluctuations in quantum wires,'' Phys. Rev. Lett. **77**, 4612–4615 (1996).

[18]W. A. de Heer, S. Frank, and D. Ugarte, ''Fractional quantum conductance in gold nanowires,'' Z. Phys. B **104**, 468–473 (1997).

[19]J. L. Costa-Krämer, N. García, P. García-Mochales, and P. A. Serena, ''Nanowire formation in macroscopic metallic contacts: Quantum Mechanical conductance [by] tapping a table top,'' Surf. Sci. **342**, L1144–L1149 (1995).

[20]Stefan Frank, Phillippe Poncharal, Z. L. Wang, and Walt A. de Heer, ''Carbon Nanotube Quantum Resistors,'' Science **280**, 1744–1746 (1998).

[21]E. A. Montie, E. C. Cosman, G. W. 't Hooft, M. B. van der Mark, and C. W. J. Beenakker, ''Observation of the optical analogue of quantized conductance of a point contact,'' Nature (London) **350**, 594–595 (1991).

[22]E. Abrahams, P. W. Anderson, D. C. Licciardello, and T. V. Ramakrishnan, ''Scaling theory of localization: Absence of quantum diffusion in 2D,'' Phys. Rev. Lett. **42**, 673–676 (1979).

[23]S. V. Kravchenko, Whitney E. Mason, G. E. Bowker, J. E. Furneaux, V. M. Pudalov, and M. D'Iorio, ''Scaling of an anomalous metal–insulator transition in a 2D system in Si at $B=0$,'' Phys. Rev. B **51**, 7038–7045 (1996); S. V. Kravchenko, D. Simonian, M. P. Sarachik, Whitney E. Mason, and J. E. Furneaux, ''Electric field scaling at a $B=0$ M–I transition in 2D,'' Phys. Rev. Lett. **77**, 4938–4941 (1996). A follow-up paper organizes some earlier data in complementary fashion: Dragana Popovic, A. B. Fowler, and S. Washburn, ''Metal–insulator transition in 2D: Effects of disorder and magnetic field,'' *ibid.* **79**, 1543–1546 (1997).

[24]See, for example, J. R. Hook and H. E. Hall, *Solid State Physics* (Wiley, Chichester, 1991), 2nd ed., pp. 400–412. Good treatments are given by R. E. Prange in *The Quantum Hall Effect* (Springer-Verlag, New York, 1990), 2nd ed., pp. 22–30 and in the early part of an article by L. J. Challis, ''Physics in less than three dimensions,'' Contemp. Phys. **33**, 111–127 (1992). Several topics treated in the present paper overlap the subject matter of the Challis article.

[25]I call attention to a more extensive treatment of various elements of theoretical background than is given here, in an article by J. P. Eisenstein, ''The quantum Hall effect,'' Am. J. Phys. **61**, 179–183 (1993). An even more complete treatment of theoretical background for a number of aspects of the IQHE is given in the very nice review paper by H. Aoki, ''Quantised Hall Effect,'' Rep. Prog. Phys. **50**, 665–730 (1987).

[26]See J. R. Hook and H. E. Hall in Ref. 24. In particular, Ref. 25 of their book, pp. 402–412.

[27]See J. R. Hook and H. E. Hall in Ref. 24. In particular, Ref. 25 of their book, p. 408.

[28]D. B. McWhan, A. Menth, J. P. Remeika, W. F. Brinkman, and T. M. Rice, ''Metal–insulator transitions in pure and doped V_2O_3,'' Phys. Rev. B **7**, 1920–1931 (1973).

[29]N. F. Mott, *Metal–Insulator Transitions* (Taylor & Francis, London, 1990), 2nd ed., pp. 36–39.

[30]See, e.g., Judy R. Franz, ''Metal–insulator transition in expanded alkali metal fluids and alkali metal–rare gas films,'' Phys. Rev. B **29**, 1565–1574 (1984).

[31]See, e.g., Shuichi Ishida and Eizo Otsuka, ''Galvanomagnetic properties of *n*-type InIb at low temperatures. II. Magnetic field-induced Metal–Nonmetal Transition,'' J. Phys. Soc. Jpn. **43**, 124–131 (1977).

[32]The fractional effect has been brought into high public prominence by the award of the 1998 Nobel Prize in Physics to experimentalists Horst Störmer and Daniel Tsui for its discovery and theorist Robert Laughlin for his elucidation of a theoretical model for the effect. A full treatment of the fractional QHE is given in the monograph *The Quantum Hall Effect*, edited by Richard E. Prange and Steven M. Girvin (Springer-Verlag, New York, 1990), 2nd ed. Comment: The present author finds it curious that the new plateaus associated with fractional quantum numbers appear innocently in the experimental data as though only a refinement of the integral plateaus. But it then turns out that they require a significantly more elaborate theoretical model for their explanation.

[33]See the chapter entitled ''Experimental Aspects and Metrological Application,'' by Marvin E. Cage, in the Prange and Girvin volume, Ref. 5, for a discussion of this fascinating dividend stemming from discovery of the QHE.

[34]The pathway to setting a local standard value of the ohm in terms of the experimental value of the Klitzing constant, R_K, is described in a paper by B. N. Taylor and T. J. Witt, ''New international electrical reference standards based on the Josephson and Quantum Hall effects,'' Metrologia **26**, 47–62 (1989).

[35]J. E. Furneaux and T. L. Reinecke, ''Novel features of quantum Hall plateaus for varying interface charge,'' Phys. Rev. B **29**, 4792–4795 (1984).

[36]Most Hall effect measurements have been made with samples and electrical contacts arranged in some variation of the scheme shown in Fig. 1(b)—often loosely referred to as a ''Hall bar.'' While much less frequently used, the circular configuration known as the ''Corbino disc'' provides an alternate arrangement, with important differences in electrical characteristics. Recent measurements using the Corbino disc geometry, to be referenced subsequently, have provided valuable experimental information to supplement the Hall bar data. The Corbino disc configuration and its use is briefly described in Appendix B.

[37]The reader may find it of great value to refer to a recent article in this journal. (''Electric potential in the classical Hall effect: An unusual boundary value problem,'' by Matthew J. Moeller, James Evans, Greg Elliott and Martin Jackson, Am. J. Phys. **8**, 668–677 (1998).)

[38]A. H. MacDonald, T. M. Rice, and W. F. Brinkman, ''Hall voltage and current distribution in an ideal 2D system,'' Phys. Rev. B **28**, 3648–3651 (1983).

[39]P. F. Fontein, J. A. Kleinen, P. Henriks, F. A. P. Blom, J. H. Wolter, H. G. M. Lochs, F. A. J. M. Driessen, L. J. Giling, and C. W. J. Beenaker, ''Spatial potential distribution in GaAs/Al_xGa_{1-x}As heterostructures under Quantum Hall conditions, studies with the linear electro-optic effect,'' Phys. Rev. B **43**, 12090–12093 (1991).

[40]Note that the direction of flow of these edge currents, formed from the skipping orbits, is such as to oppose the diamagnetic effect of cyclotron orbits within the sample. In a simple classical picture, these countervailing effects cancel one another out. But Landau, in 1930, showed that a correct quantum mechanical calculation for a free electron system recovers a net diamagnetism—which happens to be in magnitude equal to one-third of the Pauli spin susceptibility of the free electron system. A full quantum-mechanical treatment of this Landau diamagnetism is given in *The Theory of Metals*, by A. H. Wilson (Cambridge University Press, Cambridge, 1958), pp. 160–167 (and, no doubt, in other standard second-level solid state physics treatments.)

[41]R. B. Laughlin, ''Quantized Hall conductivity in two dimensions,'' Phys. Rev. B **23**, 5632–5633 (1981).

[42]B. I. Halperin, ''Quantized Hall conductance, current-carrying edge states, and the existence of extended states in a two-dimensional disordered potential,'' Phys. Rev. B **25**, 2185–2190 (1982). Halperin's representation of the Laughlin argument uses a physical model in which the sample is in the form of a flat, circular ''washer.'' The edge currents flow smoothly in circular paths at the inner and outer edges of the washer. This configuration is, in fact, a variant of the Corbino disc. See Appendix B for a discussion of the Corbino disc sample configuration.

[43]Reference 4, pp. 566–570.
[44]M. Büttiker, ''Absence of backscattering in the Quantum Hall effect in multiprobe conductors,'' Phys. Rev. B **38**, 9375–9389 (1988).
[45]R. J. F. van Haren, F. A. P. Blom, and J. H. Wolter, ''Direct Observation of Edge Channels in the Integer Quantum Hall Regime,'' Phys. Rev. Lett. **74**, 1198–1201 (1995).
[46]B. Jeanneret, B. D. Hall, H.-J. Bühlmann, R. Houdré, M. Ilegems, B. Jeckelmann, and U. Feller, ''Observation of the integer Quantum Hall Effect by magnetic coupling to a Corbino Ring,'' Phys. Rev. B **51**, 9752–9756 (1995).
[47]See Beenakker and Van Houten, Ref. 6, pp. 172–177, for extended discussion of the model which combines edge channels with the effects of nonconducting islands.
[48]S. H. Tessmer, P. I. Glicofridis, R. C. Ashoori, L. S. Levitov, and M. R. Melloch, ''Subsurface charge accumulation imaging of a quantum Hall liquid,'' Nature (London) **392**, 51–54 (1998).
[49]Dmitri B. Chklovskii and Patrick A. Lee, ''Transport properties between Quantum Hall plateaus,'' Phys. Rev. B **48**, 18060–18078 (1993).
[50]M. E. Cage, ''Current distributions in Quantum Hall effect devices,'' J. Res. Natl. Inst. Stand. Technol. **102**, 677–691 (1997); M. E. Cage and C. F. Lavine, ''Potential and current distributions calculated across a Quantum Hall effect sample at low and high currents,'' *ibid.* **100**, 529–541 (1995).
[51]G. Ebert, K. von Klitzing, K. Ploog, and G. Weimann, ''2D magneto-quantum transport in GaAs–$Al_xGa_{1-x}As$ heterostructures under non-Ohmic conditions,'' J. Phys. C **16**, 5441–5448 (1983).
[52]An extended discussion of the conditions necessary for observation of various electron quantum interference effects is given by Richard A. Webb and Sean Washburn, ''Quantum interference fluctuation in disordered metals,'' Phys. Today **41** (12), 41–55 (1988).
[53]G. Bergmann, ''Weak localization in thin films,'' Phys. Rep. **107**, 1–58 (1984).
[54]R. Corey, M. Kissner, and P. Saulnier, ''Coherent backscattering of light,'' Am. J. Phys. **63** (6), 560–564 (1995).
[55]*Analogies in Optics and Microelectronics*, edited by W. Van Haeringer and D. Lenstra (Kluwer, Dordrecht, 1990).
[56]R. A. Webb, S. Washburn, and C. P. Umbach, ''Experimental study of nonlinear conductance in small metallic samples,'' Phys. Rev. B **37**, 8455–8458 (1988).
[57]P. A. Lee, A. D. Stone, and H. Fukuyama, ''Universal conductance fluctuations in metals: Effects of finite temperature, interactions and magnetic field,'' Phys. Rev. B **35**, 1039–1070 (1987).
[58]Reference 6, pp. 91–98.
[59]O. M. Corbino, ''Bahn der Ionen in Metallen,'' Phys. Z. **12**, 561–568 (1911). This circular configuration, infrequently used in the decades since the original paper, eliminates contact effects if the current is driven by an ac source, with Hall voltage picked up by a search coil placed concentrically around the disc. (Note: The journal which published Corbino's paper *is* Physikalische Zeitschrift, *not* the more familiar Zeitschrift für Physik. This reference is included for reasons of historical interest. Knowledge of its content is not particularly relevant to uses of this configuration in studying the QHE.)

SOFTWARE LIMITATIONS

For all the achievements made possible by computers, there is growing concern in the engineering-design community that there are numerous pitfalls that can be encountered in using software packages. All software begins with some fundamental assumptions that translate into fundamental limitations, but these are not always displayed prominently in advertisements. Indeed, some of the limitations of software might be equally unknown to the vendor and to the customer. Perhaps the most damaging limitation is that software can be misused or used inappropriately by an inexperienced or overconfident engineer.

Henry Petroski, ''Failed Promises,'' American Scientist **82**(1), 6–9 (1994).